國 立 交 通 大 學

電信工程學系

博 士 論 文

微帶線高指向性耦合結構之研究與其應用

Research and applications of microstrip coupled line structure with high directivity

研究生：王士鳴 (Shih-Ming Wang)

指導教授：張志揚 (Chi-Yang Chang)

中 華 民 國 九 十 四 年 九 月

微帶線高指向性耦合結構之研究與其應用

學生: 王士鳴　　　指導教授: 張志揚 博士

國立交通大學

電信工程學系

摘要

本論文主要在研究高指向性微帶結構及其應用。在論文的第一部份,我們提出彎折式耦合線結構,其可有效地對偶模波速進行加速,在適當設計下,可使奇偶模波速相等,而使耦合器具有高指向性的效能。我們先設計出一個在極窄頻範圍內可達成極高指向性的耦合器,再經由一些變化,可將其改變成一個在大頻寬範圍內皆具有高指向性的耦合器。我們也將此結構應用在半波長帶通濾波器上,並且成功地抑制了第一次諧振通帶。此結構的設計與合成過程在論文中有完整詳細的說明。在論文的第二部份,提出了一種設計架構,能有效縮小微帶平行弱耦合器的面積,並保有高指向性的效能。

Research and applications of microstrip coupled line structure with high directivity

Student: Shih-Ming Wang   Advisor: Dr. Chi-Yang Chang

Department of Communication Engineering

National Chiao Tung University

Abstract

This dissertation presents the research and applications of microstrip coupler with high directivity. In the first part, we proposed a meandered parallel-coupled line. It can speed up the even-mode phase velocity and make the modal phase velocities to be equal in microstrip structure. Therefore, we can get a good directivity in microstrip parallel-coupled coupler. With proper design, we can get an ultra high directivity in a narrow band or get a high directivity performance over broad bandwidth. We also apply the proposed structure to a half wavelength band pass filter and successfully cancel the first spurious passband. All the synthesis procedures of the proposed structure are described in detail. The second part presents a solution for miniaturizing microstrip loose coupler with high directivity.

誌謝

　　首先要感謝張志揚教授在這幾年來辛勤與耐心的指導，其觀念啟發以及適當的協助帶我走出研究上的迷惘，也使本研究得以完成。另外也感謝口試委員陳俊雄教授、吳瑞北教授、鍾世忠教授、郭仁財教授與楊正任教授對本研究所給予的指正與建議。

　　這裡還要特別感謝微波薄膜實驗室的學弟謝明諭與紀鈞翔，無論是在研究討論或是生活減壓上給予的幫助。另外，對於曾幫助過我的實驗室學長、姐、弟、妹在此一併誌謝。

　　接下來，還要感謝我在美國交換研究期間的指導教授林仁山教授對我在待人與研究精神上的另類啟發。也感謝在美國認識，曾給予我各項協助與研究打氣的好朋友們，讓我在美國的生活充實且快樂。

　　最後在此感謝我的家人與女友昱璇在我背後默默地給予我在經濟上與精神上的支持與鼓勵，謝謝你們！

士鳴

2005 年九月於台灣新竹

Contents

List of Tables

List of Figures

Chapter 1

Introduction

Microwave transmission lines are normally classified as two types: (1) to carry information or energy from one point to another; (2) as circuit element for passive circuits like couplers, baluns, filters, resonators, and impedance transformers. In microwave circuits, passive elements mainly consist of distributed type and employ transmission line sections and waveguides in different configurations and to achieve the desired specifications. The functionality is largely achieved by the use of coupled transmission lines. In which, microstrip coupled lines are popular due to the low cost and easy fabrication. However, the inherent disadvantage of poor directivity destroys the performances of the coupler itself and limits the feasibility in various extended applications. In this chapter, we briefly describe the original of coupled lines, the significance of high directivity, previous works for directivity improvement, and our proposal and contributions.

1.1 Brief History

The exact beginnings of directional couplers using parallel wires are not clear. Such couplers were used for various applications before any of the modern theories or design data were available. The first directional coupler using a quarter-wave-long two-wire configuration, U.S. Patent 1,615,896, entitled "High Frequency Signaling System" [1] was filed in 1922 and granted in 1927 to Herman A. Affel, and assigned

to American Telephone and Telegraph Company. Affel refers to a "loop antenna", which is shown in Figure 1.1 consists of a two-wire transmission line quarter-wavelength long, with a resistive termination at one end and a detector at the other end. This quarter-wavelength line which was called loop antenna is parallel to another longer two-wire transmission line, and could work like a directional coupler at midband of properly design. However, it is not explicitly referred to as a directional coupler.

A clear description with formulas of a TEM-mode quarter-wavelength parallel-line backward coupler was filed in U.S. Patent 2,606,974, entitled "Directional Coupler" [2] in 1946, and granted in 1952 to Harold A. Wheeler, being assigned to Hazeltine Research, Inc. The cover is reproduced here as Figure 1.2. Wheeler states that it was used in 1944 at the Hazeltine laboratory.

Directional couplers using planar TEM lines such as coupled striplines were developed in the mid-1950s. Numerous papers were published in the 1950s and 1960s describing the theory, design, fabrication, and measured data for the TEM-line edge-coupled directional couplers and significant contributions were made in the development of planar couplers. These couplers can provide coupling in the 8- to 40-dB range. Early works on these homogeneous couplers can be found in [3]-[4]. These couplers are also known as backward couplers because the coupled wave on the secondary line travels in the opposite direction compared with the incident wave on the primary line when excited with a microwave signal.
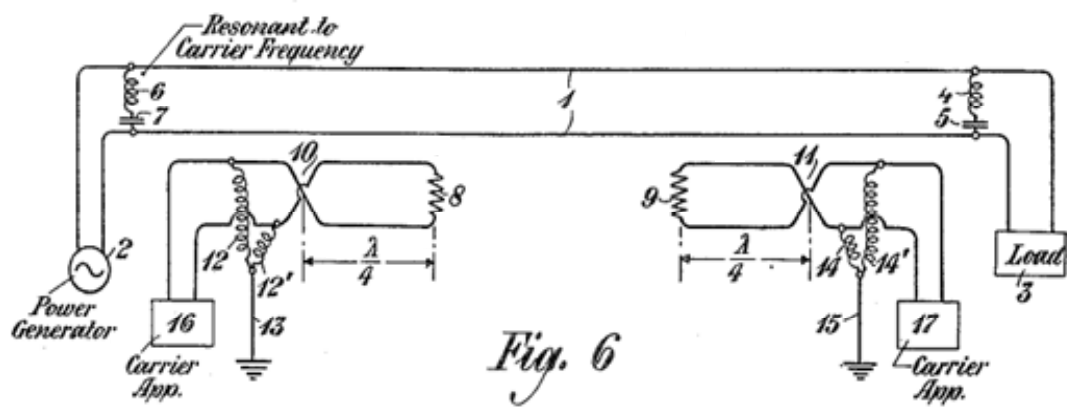
Figure 1.1   The first directional coupler using a quarter-wave-long two-wire configuration.
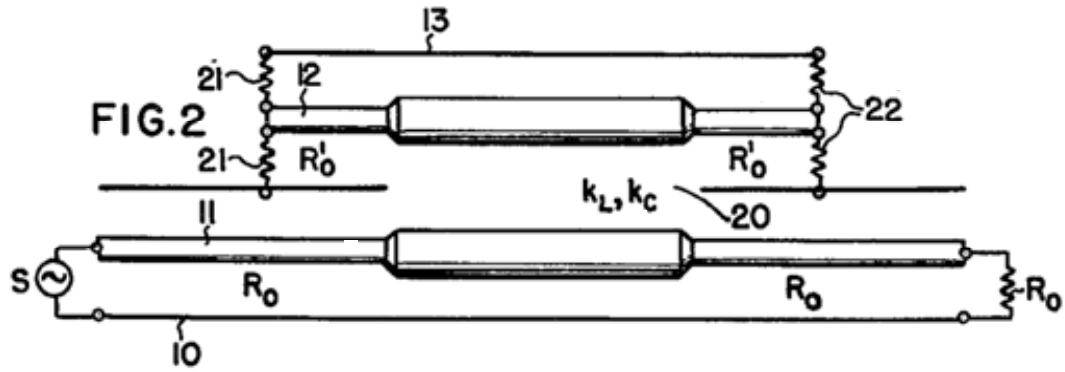
Figure 1.2   The first TEM-mode quarter-wavelength parallel-line backward coupler with clear description with formulas.

1.2 Research Motivations

Microstrip coupling structure has become very popular due to insensitivity to fabrication tolerance and simple synthesis procedures. Its planar structure allows laying solid-state devices and lumped elements on its surface. Microstrip coupling structure can be used to design many various microwave circuits, such as directional coupler, edge-coupled line filter, balun, delay line, dc block, interdigital capacitor, spiral inductor, coupled-line impedance transformer, and spiral transformer. And it also frequently appears in high-speed digital signal printed circuit board and in many microwave measurement systems.

However, based on its semi-open structure, the electromagnetic field distributes in both air and dielectric region, and the propagation mode is quasi TEM. Due to the inhomogeneous material that results the odd-mode phase velocity commonly faster than the even-mode value, in another word, that causes the odd-mode transmission phase smaller than the even-mode value. The inequality of modal phase velocities (and transmission phases) will degrade the isolation or directivity performance of the microstrip coupled-line structure. The performances of many of the microwave circuits mentioned above degrade because of poor directivity. For a backward-wave directional coupler, the coupling value might change, as the coupler isolation is not very good and in the mean time the coupler is not well terminated. For a Machand type balun, the balance of amplitude and/or phase degrade due to poor directivity. For a coupled-line bandpass filter, extra spurious passband appears and it might make the upper stopband performance get worse. For some of other circuits, the parasitic effects might cause undesirable performances. Therefore, a microstrip coupled-line structure with good isolation is important for various microwave circuits design.

The second problem encountered in the microstrip coupled-line coupler is that as the coupling gets loose, two lines of convention coupler becomes wider spaced. That makes the coupler not only occupies more circuit area but also has very poor directivity. Because of the large line spacing, the capacitor compensation of phase velocity becomes very difficult. In addition, in order to get a near-constant coupling over a wider frequency bandwidth, a multisection coupler that consists of a number of single-section couplers with tight and loose coupling is commonly used. However, the different coupling has different spacing between the two coupled lines for each section of coupler. This means that the discontinuities certainly exist in the junctions of different single-section couplers, even if the small lengths of tapered transmission lines are used. In higher frequency, these discontinuities will produce extra reactance and lengths and then degrade the input matching and directivity. Therefore, a loose coupler with narrower coupled-line spacing is needed for reducing the discontinuities. Besides, the directivity of a single-section coupler is more important in multisection coupler application. The unequal phase velocities will get poor directivity and make the coupling to be inaccurate especially when the whole coupled line length get longer. So, a loose coupler with narrower coupled-line spacing and high directivity is necessary for a multisection coupler.

The purpose of this research is to find some methods to solve the above-described problems.
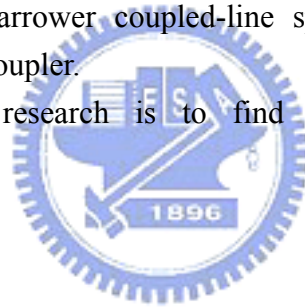
1.3 Literature Survey

For improving the directivity of the microstrip coupled-line coupler, there are many early works are proposed to equalize or compensate of unequal modal phase velocities (and modal transmission phases). Basically, methods to solve this problem can be summarized in three major groups. The first method is shown in Figure 1.3. By adding single or multiple lumped elements at the end or the center of the coupler, the odd-mode phase velocity slows down due to the raise of the odd-mode effective dielectric constant [5]-[9]. On the other hand, the lumped elements are nearly invisible in the even mode. The initial synthesis procedures and the achievable coupling range of this compensated method are the same as conventional coupler. Moreover, it is effective to get high directivity in a wide bandwidth. However, the value of lumped component should be calculated and length of coupled section should be shortened due to the odd-mode phase velocity slows down. Although [5]-[7] provide the formulas for calculating the value of lumped element and shortened length, in practice, the available lumped element value usually does not meet the exact value and the lumped component usually shows parasitic effects as the frequency goes high.

Distributed component is, therefore, a good solution to implement the lumped element in high frequency.
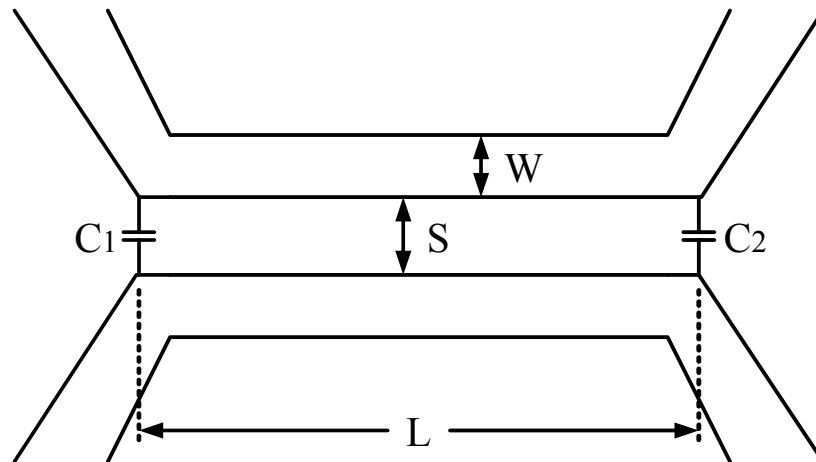
Figure 1.3   Lumped capacitor compensation of microstrip coupler.

The second method is shown as Figure 1.4. By placing one or more additional dielectric layers with proper thickness and dielectric constant on top of microstrip coupler, the odd-mode phase velocity can be slowed down due to the increase of odd-mode effective dielectric constant, and can be equaled to the even-mode value [10]-[15]. This thought is straight forward and it can shorten the circuit size by show-wave effect. Furthermore, it makes the realization of tight coupling easier with the same lines spacing. However, it's not a planar structure anymore and adding any additional material needs extra cost and process. Moreover, due to the variation of dielectric environment, the line width and line spacing are different from the initial dimensions of microstrip coupler and need to be recalculated. Unfortunately, there are no mature synthesis formulas for various dielectric environments. To obtain most of the dimensions require some special design charts and need electro-magnetic field analysis to calculate the characteristics of the proposed special structure. This kind of design is more complicated and time-consuming. The most important drawback is that the design results fit case-by-case and common solution is difficult to obtain.

The third method is shown in Figure 1.5 that the inner edges of a pair of microstrip lines are changed to wiggle or serpentining or slot shape [16]-[20]. Since most of the odd-mode current is propagated along the inner edge, the effective propagating length of the odd-mode signal is increased so that the propagating phase of odd-mode can be equaled to that of the even-mode signal. The circuit structure is pure planar and the slow wave-like effect can effectively shorten the physical length of the circuit. However, the design begins with Fourier transform analysis, and the

synthesized structure is optimized using iterative techniques [20]. These steps cannot be implemented in standard simulators, and the whole process is rather time-consuming. Besides, the unsmooth inner edge not only makes the high order propagating mode easily to be excited but also increases the insertion loss. Moreover, the odd-mode inductance per unit length increases, as the variation of inner edge gets more drastic. That means the odd-mode characteristic impedance increases and results in a looser coupling as comparing to the conventional coupled lines with the same line spacing.

For improving the directivity of loosely coupled microstrip lines, few works have been done on this topic. As [21] indicates, it's not appropriate to add lump capacitor on the two ends of a loose coupler due to the wide coupled line spacing and only very small compensated capacitance is needed. Conventional lump capacitor is hard to get exact and such a low capacitance value. In the contrary, interdigital capacitor is good for this kind of application, because it is easier to fit the wide coupled-line spacing and to get exact and lower capacitance.

There are some previous works for loose coupler design in microstrip structure, most of them are based on broadside coupling with some slots or apertures in the substrate but no one is based on edge coupling scheme.
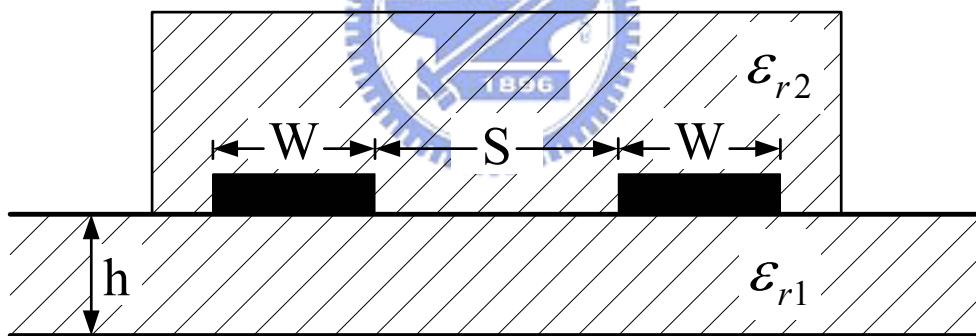
Figure 1.4   Parallel-coupled microstrip with dielectric overlay compensation.
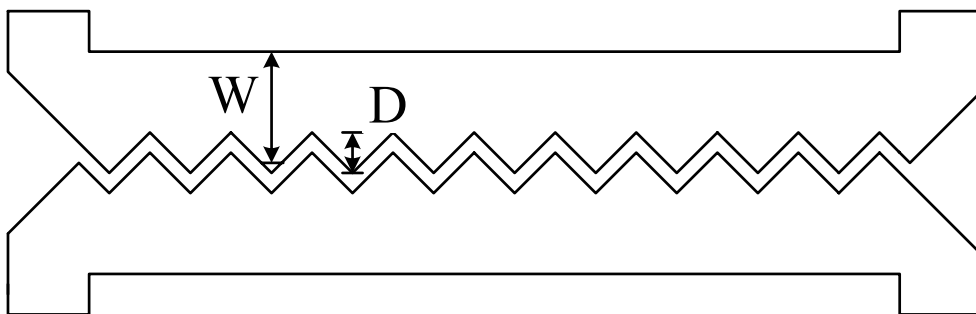
Figure 1.5   Wiggly two-line coupler.

1.4 Contribution

Comparing to the various methods for directivity improvement described in section 1.3, this dissertation proposes the structure of meandered parallel-coupled line. The even-mode phase velocity can be speeded up by meandering the parallel-coupled line. Proper meandering equals the even- and the odd-mode phase velocities and achieves high directivity. By the single section meandered parallel-coupled lines, we can locate high directivity performance at any narrow frequency band that we want. Furthermore, the frequency band with high directivity can be wider by dividing the coupled line in to multiple sections of cascaded meandered parallel-coupled lines. In addition, the proposed structure, based on the characteristic of meandering, can effectively miniaturize the circuit for all of its applications, especially in higher order filter design. In practical fabrication, no addition component, material, and process are needed, thus, low fabrication cost can be kept.

In another part of this dissertation, a miniaturized high directivity loose microstrip coupler is proposed. We place a grounded strip between the two parallel-coupled lines to block the coupling and place two interdigital capacitors in both ends of the coupler to improve the directivity. The design procedures and consideration will be discussed in detail.

1.5 Chapter outline

In this dissertation, Chapter 1 is the introduction, which describes the original of parallel-coupled lines and the importance of the directivity. A brief description of the proposed methods is provided with comparison of various previous works. Chapter 2 describes the inherent characteristics and disadvantages of microstrip parallel-coupled lines, and derives the scattering parameters to obtain the necessary conditions for high directivity in the basis of Quasi-TEM mode. Chapter 3 describes the motivation of using the meandered parallel-coupled lines and the characteristics of this kind of parallel-coupled line. Moreover, it also describes the procedures to synthesis the proposed meandered parallel-coupled lines by commercial CAD tools in detail. Then, based on the proposed structure, two couplers are designed and demonstrated with narrow-band and wide-band high directivity performance, respectively. Chapter 4 uses the characteristics of the proposed meandered parallel-coupled lines to design a bandpass filter not only eliminating the spurious passband near twice of the center frequency but also drastically shrinking the circuit size. In this chapter, the design procedures and information are described in detail for this kind of filter. Chapter 5

describes the design of the miniaturized loosely coupled parallel-coupled line coupler with high directivity. Chapter 6 gives the conclusion.

Chapter 2

Theory of the microstrip parallel coupled line coupler
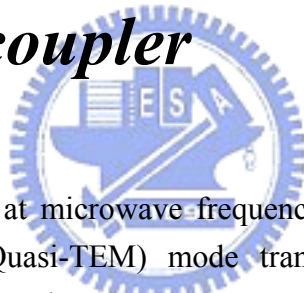
Transmission lines used at microwave frequencies can be briefly divided into two categories: TEM (or Quasi-TEM) mode transmission lines and non-TEM transmission lines. When a signal propagates on a microstrip structure, because the electromagnetic fields are distributed in an inhomogeneous material, the propagation mode is Quasi-TEM. For a symmetric TEM or Quasi-TEM coupled transmission lines, the determination of important electrical characteristics (such as modal characteristic impedances and phase velocities) of coupled lines reduces to finding the modal capacitances associated with the structure and excitation mode. This chapter discusses the general characteristics of symmetric microstrip parallel coupled lines and also gives the design equations. In addition, the scattering parameters of microstrip parallel coupled lines based on Quasi-TEM mode are derived without the constrain of equal modal phase velocities and the necessary conditions for high directivity is also discussed. Finally, some practical suggestions are given for designing a high-directivity microstrip coupler.

2.1 The characteristic of microstrip parallel coupled line

When two conductor lines close to each other, the electromagnetic waves

propagating on each line interferes each other. Coupler is an application based on this scheme. The physical structure of a microstrip coupler is shown in Figure 2.1, where h and ε_r are the thickness and dielectric constant of substrate, respectively, t is the thickness of conductor, W is the coupled line width, S is the spacing between coupled line, and L is coupled line length. Figure 2.2 is the cross sectional view of the microstrip coupled lines. The structure can be analyzed by even- and odd-mode excitation. The even-mode electrical field distribution of one-half of the structure is shown in Figure 2.3(a). In this case, both lines are driven in phase from equal source of equal impedance and voltage, and the impedance from one line to ground in even-mode excitation can be defined as the even-mode characteristic impedance, Z_{0e}. Since the electrical fields between both coupled lines are parallel to the symmetric plane of the circuit, the normal component of the electric field at PP' plane is zero. It can be imaged a magnetic wall (M-wall) exists on the symmetric plane PP' and it is effectively an open-circuit on that plane. The even-mode capacitance of either of the coupled lines, which can be represented as shown in Figure 2.3(b), is given by,

$$C_e = C_p + C_f + C_{fe} \tag{2.1}$$

The capacitance that results from the electrical field in the region directly below the strip is known as the parallel-plate capacitance C_p, while that resulting from the fringing fields in the outer edge is known as the fringing capacitance C_f. C_{fe} means the fringing capacitance in the inner edge of coupled lines, which is different from C_f, because the inner edge has a M-wall near by.

The electrical field distribution of one-half of the coupled structure is shown in Figure 2.3(c) for odd-mode excitation. In this case, both lines are driven out of phase from equal source of equal impedance and voltage, and the impedance from one line to ground in odd-mode excitation can be defined as the odd-mode characteristic impedance, Z_{0o}. Since the electrical fields between both coupled lines are perpendicular to the symmetric plane of the circuit, it can be imaged an electric wall (E-wall) exists on the symmetric plane PP' and the voltage on it is zero. Because PP' is an E-wall the tangential electric field on it should be zero. The odd-mode capacitance of either of the coupled lines is given by

$$C_o = C_p + C_f + C_{fo} \tag{2.2}$$

where C_{fo} denotes the fringing capacitance from the inner edges of the coupled lines,

which is assumed to consist of two capacitances C_{ga} and C_{gd} in parallel; that is,

$$C_{fo} = C_{ga} + C_{gd} \qquad (2.3)$$

where C_{ga} and C_{gd} are the capacitances corresponding to the fringing field between the inner edges exist in the air and dielectric regions, respectively.
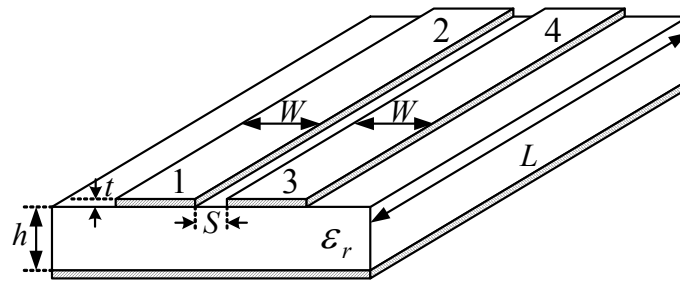
Figure 2.1   The structure of microstrip coupler.

Plane of Symmetry
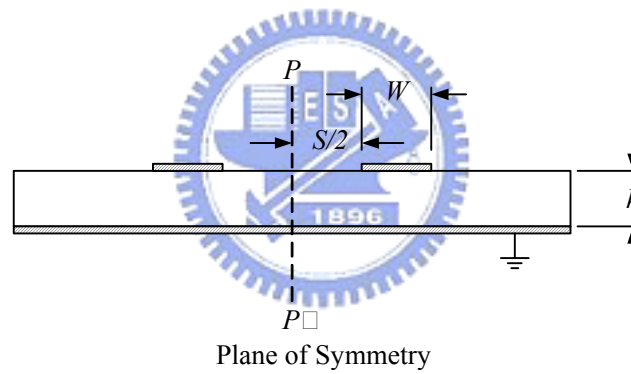
Figure 2.2   Cross section of symmetrical microstrip coupler.

Magnetic
Wall

(a)

(b)

Magnetic
Wall

(c)

Electric
Wall

(d)
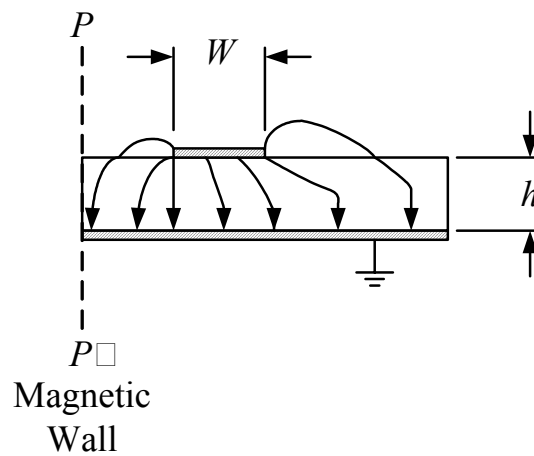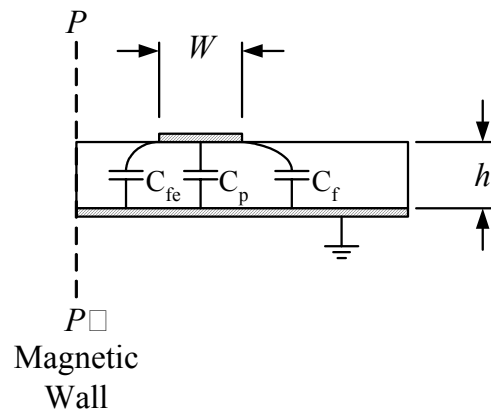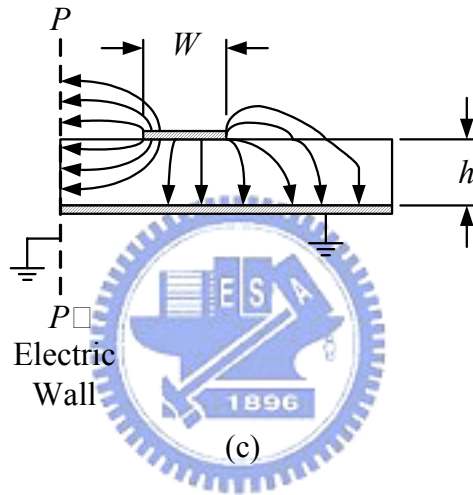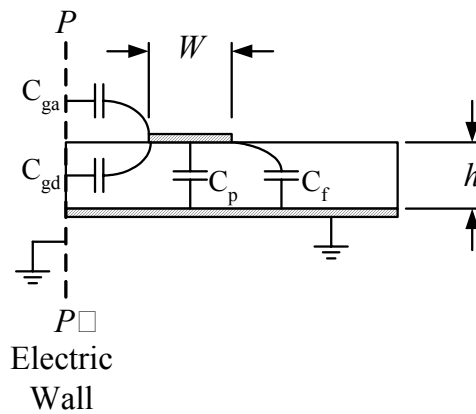
Electric
Wall

Figure 2.3   (a) The electrical field distribution and (b) capacitance representation of one-half of the structure for even-mode excitation, (c) The electrical field distribution and (d) capacitance representation of one-half of the structure for odd-mode excitation.

The definitions of the even- and the odd-mod effective dielectric constant are

$$\varepsilon^e_{r\_eff} = c^2 / V^e_p{}^2 \tag{2.4a}$$

$$\varepsilon^o_{r\_eff} = c^2 / V^o_p{}^2 \tag{2.4b}$$

where c is the speed of light in free space, and V^e_p and V^o_p are the even- and the odd-mode phase velocity, respectively. In Figure 2.2, the effective dielectric constants take into account the relative distribution of electric field in the various regions of the inhomogeneous medium. Besides, the effective dielectric constants are a function of frequency and strictly speaking should be evaluated using equation (2.4) where the phase velocity is compute by using some rigorous method based on Maxwell's equations. However, on the quasi-static assumption, the even- and odd-mode effective dielectric constant can be defined as fellows:

$$\varepsilon^e_{r\_eff} = C_e / C_{e1} \tag{2.5a}$$

$$\varepsilon^o_{r\_eff} = C_o / C_{o1} \tag{2.5b}$$
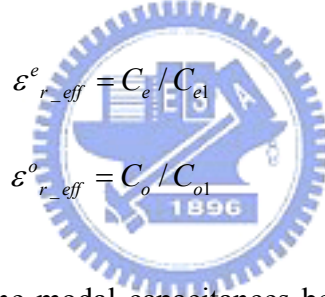
where C_{e1} and C_{o1} denote the modal capacitances between the same conductor in a homogeneous dielectric medium of unity dielectric constant. In order to get the sense for the even- and odd-mode dielectric constant, let us refer to Figure 2.3 (a) and (c), which show the even- and odd-mode electrical field distributions of a microstrip parallel coupled line. The figures indicate that the relative E-field distributions in air and substrate region are different for the two modes, and the odd-mode electrical field has more relative distributions in the air region. It implies that the $\varepsilon^o_{r\_eff}$ is smaller than $\varepsilon^e_{r\_eff}$ and V^o_p is faster than V^e_p by equation (2.4).

The transmission phases of both modes are

$$\theta_e = \frac{\omega}{V^e_p} L \tag{2.6a}$$

$$\theta_o = \frac{\omega}{V^o_p} L \tag{2.6b}$$

where ω is operation angular frequency, L is the physical length of the parallel

coupled line.

The even- and odd-mode characteristic impedance are given by

$$Z_{0e} = \frac{1}{C_e V^e_p} \tag{2.7a}$$

$$Z_{0o} = \frac{1}{C_o V^o_p} \tag{2.7b}$$

The detailed analysis formulas for even- and odd-mode characteristic impedance in microstrip coupled lines can refer to [22].

2.2 The necessary conditions of a high directivity coupler

Figure 2.4 is the schematic circuit of microstrip coupler. Because of symmetry, the excitation in Figure 2.4 can be decomposed into even-mode and odd-mode excitations as shown in Figure 2.5(a) and (b), respectively. In order to analysis easily, the schematic circuits on Figure 2.5(a) and (b) can be simplified as shown in Figure 2.6 (a) and (b) which are two-ports circuit with characteristic impedance Z_{0e} and Z_{0o}, transmission phase θ_e and θ_o, respectively. Since the even- and odd-mode circuits are two-port network, the ABCD matrix for the even- and odd-mode are given, respectively, by

$$\begin{bmatrix} A_e & B_e \\ C_e & D_e \end{bmatrix} = \begin{bmatrix} \cos\theta_e & jZ_{0e}\sin\theta_e \\ jY_{0e}\sin\theta_e & \cos\theta_e \end{bmatrix} \tag{2.8a}$$

$$\begin{bmatrix} A_o & B_o \\ C_o & D_o \end{bmatrix} = \begin{bmatrix} \cos\theta_o & jZ_{0o}\sin\theta_o \\ jY_{0o}\sin\theta_o & \cos\theta_o \end{bmatrix} \tag{2.8b}$$

And then transfer the ABCD matrix to scattering matrix, we obtain

$$[S_e] = \begin{bmatrix} S_{11e} & S_{12e} \\ S_{21e} & S_{22e} \end{bmatrix} \tag{2.9a}$$

$$[S_o] = \begin{bmatrix} S_{11o} & S_{12o} \\ S_{21o} & S_{22o} \end{bmatrix} \tag{2.9b}$$
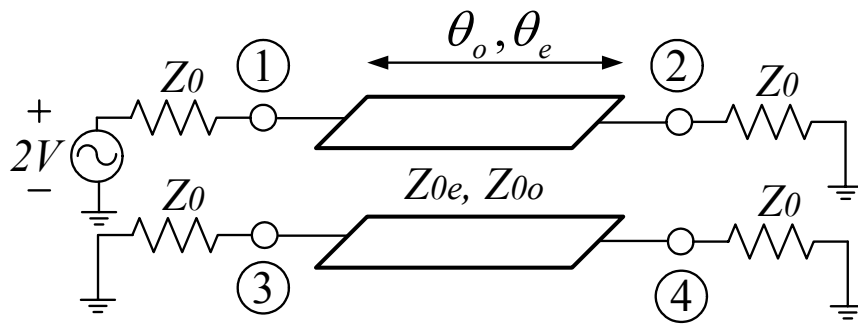
Figure 2.4　The schematic circuit of microstrip coupler.

(b)
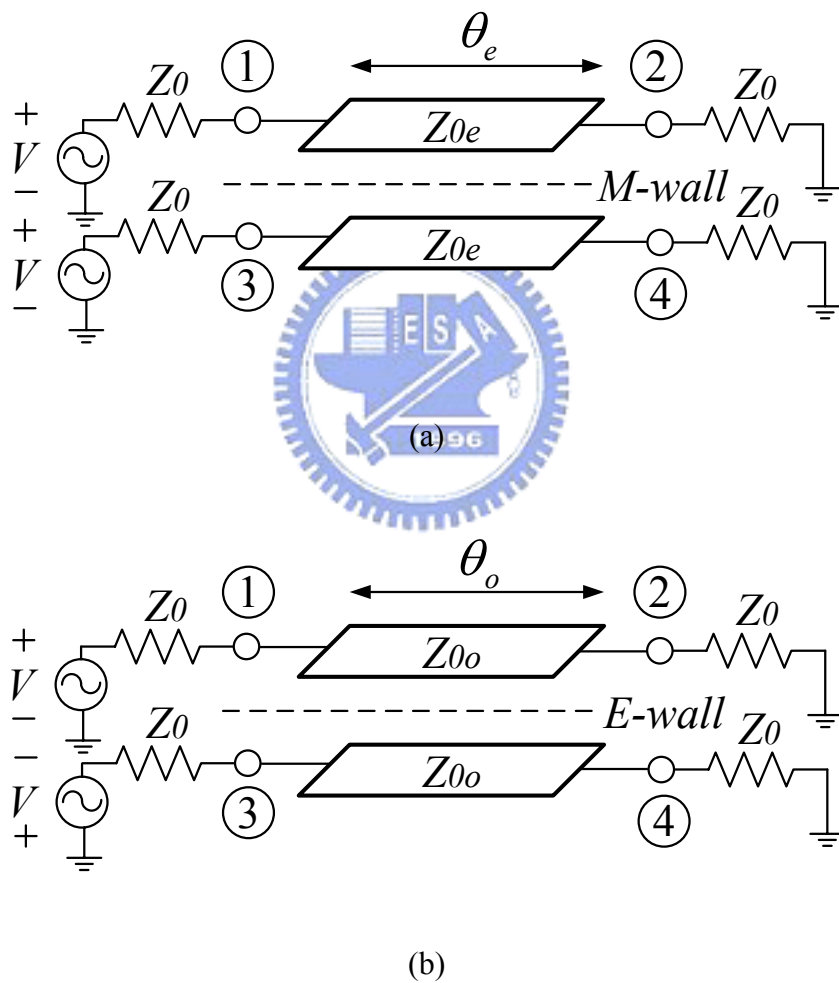
Figure 2.5　The decomposition of coupled line coupler circuit of Figure 2.3 into even-mode and odd-mode excitations. (a) Even mode. (b) Odd mode.

(a)

(b)
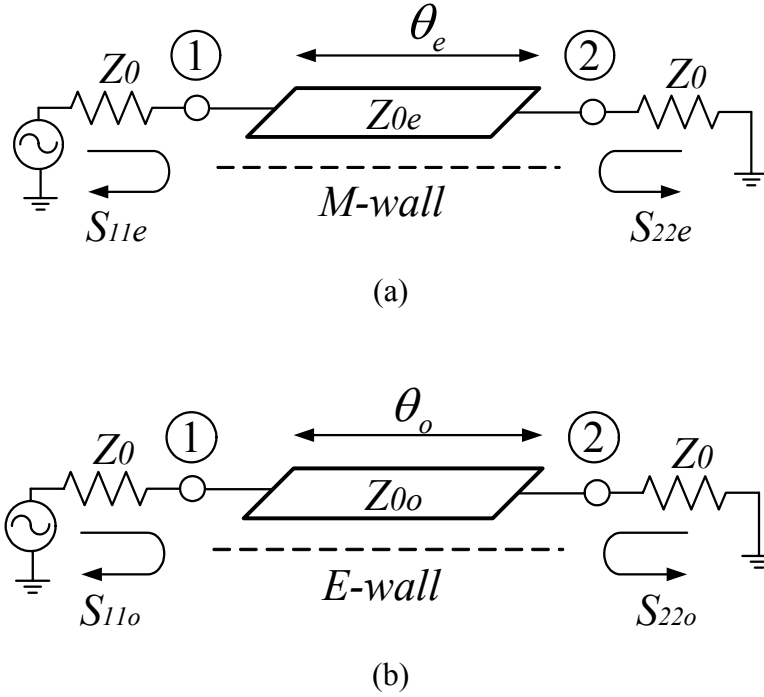
Figure 2.6   Equivalent circuit for determining scattering matrix of the (a) Even mode.
(b) Odd mode.

The 4-port scattering parameters can be determined as follows:

$$S_{11} = \frac{\left(S_{11e} + S_{11o}\right)}{2} \tag{2.10a}$$

$$S_{21} = \frac{\left(S_{21e} + S_{21o}\right)}{2} \tag{2.10b}$$

$$S_{31} = \frac{\left(S_{11e} - S_{11o}\right)}{2} \tag{2.10c}$$

$$S_{41} = \frac{\left(S_{21e} - S_{21o}\right)}{2} \tag{2.10d}$$

Since the structure of microstrip coupler is symmetric, the four scattering parameters shown in (2.10) can represent the whole scattering matrix of microstrip coupler. The equation (2.10a), (2.10b), (2.10c), and (2.10d) are the return loss, through, coupling and isolation of a coupler, respectively. Finally, the return loss of microstrip coupler in equation (2.10a) can be derived as

$$S_{11} = \frac{(Z_{0e}{}^2 Z_{0o}{}^2 - Z_0{}^4)\sin\theta_e \sin\theta_o + jZ_0 \left[(Z_0{}^2 Z_{0e} - Z_{0e}Z_{0o}{}^2)\cos\theta_e \sin\theta_o + (Z_0{}^2 Z_{0o} - Z_{0o}Z_{0e}{}^2)\cos\theta_o \sin\theta_e \right]}{[(Z_0{}^2 + Z_{0e}{}^2)\sin\theta_e - 2jZ_0 Z_{0e}\cos\theta_e][(Z_0{}^2 + Z_{0o}{}^2)\sin\theta_o - 2jZ_0 Z_{0o}\cos\theta_o]}$$

$$(2.11)$$

To make a matched coupler the numerator of equation (2.11) should be zero. We can firstly obtain the necessary condition to make the real part of numerator in equation (2.11) to be zero. That is

$$Z_0 = \sqrt{Z_{0e}Z_{0o}} \qquad (2.12)$$

With (2.12), the imaginary part of numerator in equation (2.11) can be derived as

$$(Z_{0e}{}^2 Z_{0o} - Z_{0e}Z_{0o}{}^2)\cos\theta_e \sin\theta_o + (Z_{0e}{}^2 - Z_{0o}Z_{0e}{}^2)\cos\theta_o \sin\theta_e \qquad (2.13)$$

and in microstrip coupler, the even-mode transmission phase is always larger than that of the odd mode. Thus, we can set

$$\theta = \frac{\theta_o + \theta_e}{2} \qquad (2.14)$$

$$\theta_e = \theta + \Delta\theta/2 \qquad (2.15a)$$

$$\theta_o = \theta - \Delta\theta/2 \qquad (2.15b)$$

where $\Delta\theta$ is a small phase difference because θ_e and θ_o are close to each other. Then $\cos\theta_o$, $\sin\theta_o$, $\cos\theta_e$, and $\sin\theta_e$ can be expanded as, respectively

$$\cos\theta_o = \cos\theta\cos\Delta\theta/2 + \sin\theta\sin\Delta\theta/2 \qquad (2.16a)$$

$$\sin\theta_o = \sin\theta\cos\Delta\theta/2 - \cos\theta\sin\Delta\theta/2 \qquad (2.16b)$$

$$\cos\theta_e = \cos\theta\cos\Delta\theta/2 - \sin\theta\sin\Delta\theta/2 \qquad (2.16c)$$

$$\sin\theta_e = \sin\theta\cos\Delta\theta/2 + \cos\theta\sin\Delta\theta/2 \qquad (2.16d)$$

After substituting equation (2.12) and (2.16) to equation (2.13), the imaginary part of numerator of return loss will exactly equal to

$$-2\sin\frac{\Delta\theta}{2}\cos\frac{\Delta\theta}{2}Z_0{}^2(Z_{0e} - Z_{0o}) \qquad (2.17)$$

because Z_0 and $\cos(\Delta\theta/2)$ is impossible to be zero ($\Delta\theta$ is supposed to be a small phase difference) and it's not meaningful for Z_{0e} and Z_{0o} equal in a coupler, we know $\Delta\theta=0$ is another necessary condition for $S_{11}=0$. In practical application, the S_{11} will not too bed even though the phase difference between the two modes is over 30%. That indicates $\Delta\theta=0$, in theatrically, is a necessary condition, but not a real important condition for well matching in practically.

The through of microstrip coupler in equation (2.10b) can be derived as

$$S_{21} = \frac{Z_0 Z_{0e}}{2Z_0 Z_{0e}\cos\theta_e + j(Z_0^2 + Z_{0e}^2)\sin\theta_e} + \frac{Z_0 Z_{0o}}{2Z_0 Z_{0o}\cos\theta_o + j(Z_0^2 + Z_{0o}^2)\sin\theta_o} \quad (2.18)$$

with equation (2.12) and (2.16) and ignoring the term with $\sin\Delta\theta/2$, it can be derived as

$$S_{21} = \frac{Z_0}{2Z_0\cos\theta + j(Z_{0o} + Z_{0e})\sin\theta} \quad (2.19)$$

The coupling of microstrip coupler in equation (2.10c) can be derived as

$$S_{31} = \frac{1}{2}\left(\frac{-(Z_0^2 - Z_{0e}^2)\sin\theta_e}{(Z_0^2 + Z_{0e}^2)\sin\theta_e - 2jZ_0 Z_{0e}\cos\theta_e} + \frac{(Z_0^2 - Z_{0o}^2)\sin\theta_o}{(Z_0^2 + Z_{0o}^2)\sin\theta_o - 2jZ_0 Z_{0o}\cos\theta_o} \right)$$

$$(2.20)$$

with equation (2.12) and (2.16) and ignoring the term with $\sin\Delta\theta/2$, it can be derived as

$$S_{31} = \frac{(Z_{0e} - Z_{0o})}{(Z_{0e} + Z_{0o}) - j2\sqrt{Z_{0e}Z_{0o}}\cot\theta} \quad (2.21)$$

from equation (2.21) we know that coupling is a function of θ. And when $\theta=90^\circ$, coupling can be simplified as

$$k = \frac{(Z_{0e} - Z_{0o})}{(Z_{0e} + Z_{0o})} \quad (2.22)$$

k in equation (2.22) is so called the coupling factor, which is defined as the coupling

at the center frequency for a coupler.

The isolation of microstrip coupler in equation (2.10d) can be derived as

$$S_{41} = \frac{2Z_0^2 Z_{0e} Z_{0o}(\cos\theta_o - \cos\theta_e) + jZ_0\left[Z_{0e}(Z_0^2 + Z_{0o}^2)\sin\theta_o - Z_{0o}(Z_0^2 + Z_{0e}^2)\sin\theta_e\right]}{\left[2Z_0 Z_{0e}\cos\theta_e + j(Z_0^2 + Z_{0e}^2)\sin\theta_e\right]\left[2Z_0 Z_{0o}\cos\theta_o + j(Z_0^2 + Z_{0o}^2)\sin\theta_o\right]}$$

(2.23)

with equation (2.16), the isolation of microstrip coupler can be exactly derived as

$$S_{41} = \frac{4Z_0^2 Z_{0e} Z_{0o}\sin\theta\sin\Delta\theta/2 + jZ_0 IMG}{\left[2Z_0 Z_{0e}\cos\theta_e + j(Z_0^2 + Z_{0e}^2)\sin\theta_e\right]\left[2Z_0 Z_{0o}\cos\theta_o + j(Z_0^2 + Z_{0o}^2)\sin\theta_o\right]}$$

(2.24)

where

$$\begin{aligned}
IMG &= Z_0\left[Z_{0e}(Z_0^2 + Z_{0o}^2) - Z_{0o}(Z_0^2 + Z_{0e}^2)\right]\sin\theta\cos\Delta\theta/2 \\
&\quad - Z_0\left[Z_{0e}(Z_0^2 + Z_{0o}^2) + Z_{0o}(Z_0^2 + Z_{0e}^2)\right]\cos\theta\sin\Delta\theta/2
\end{aligned}$$

(2.25)

In order to make $S_{41}=0$, we can obtain the first necessary condition from the real part of numerator in equation (2.24) is

$$\Delta\theta = 0$$

(2.26)

Based on equation (2.26), we can obtain the second necessary condition from the equation (2.25) is

$$Z_0 = \sqrt{Z_{0e}Z_{0o}}$$

(2.27)

From both necessary conditions, we know that if we want to get a good isolation, we need match the circuit well and make the odd- and even-mode transmission phases equal to each other.

The directivity of a coupler means the ratio of power flow in the desired (coupling) and undesired (isolation) coupling path. The definition is

$$D = \frac{S_{31}}{S_{41}} = \frac{\text{Coupling}}{\text{Isoaltion}} \qquad (2.27)$$

Equation (2.27) indicates that as the coupling is looser the isolation should be better to keep the directivity. The difference between the even- and the odd-mode effective dielectric constant will be larger as the coupler's substrate dielectric constant goes higher. That means the directivity will get worse when the dielectric constant of the substrate is higher. In those of the practically used microstrip substrates, the isolation is in general between -15 to -25 dB. If the coupler's coupling is designed to be looser with the same substrate, the directivity will get worse. In addition, according to the section 2.1 and equation (2.6), we know that the θ_o is smaller than θ_e in a microstrip coupler. Further, although dielectric constant is a function of frequency, the frequency effect is small and it can be regard as a constant in relatively lower frequency band (quasi-static). Therefore, from equation (2.6), we know the phase difference between the two modes will be larger for an implemented microstrip parallel coupler as the frequency increases. That causes the isolation becomes worse as the frequency increases.

Chapter 3

Analysis, design and realization of high directivity coupler with meandered parallel-coupled line

Since the microstrip parallel coupler has the inherent disadvantage of poor directivity, we fold the parallel-coupled line to improve directivity and miniaturized the circuit size at the same time. The chapter first depicts the theory and characteristics of the proposed meandered parallel-coupled line in detail and then particularly describes how to use a circuit simulator to synthesize the dimensions of the proposed structure. Finally, in order to demonstrate the validity of the proposed structure, we design a coupler with ultra high directivity within a narrow band and then improve it to be a coupler with high directivity within a broad band.

3.1 The characteristics of meandered parallel-coupled line

As mention in section 2.1 that the even-mode phase velocity of a microstrip parallel-coupled line is slower than that of the odd-mode due to inhomogeneous material. Properly increase the even-mode phase velocity is one of the compensation methods to equal the modal phase velocities and get high directivity. When we talk about the motive of the use of meandered parallel-coupled line, as shown in Figure

3.1, first, the behavior of a Schiffman section must be studied. The Schiffman section, as shown in Figure 3.2(a), is a two-port network which is formed by connecting one side of a parallel-coupled line [23]. If the interconnecting line has zero transmission phases, the relation between transmission phase ψ and coupled electrical length φ of the two-port network is determined by

$$\cos\psi = \frac{\left[\left(\dfrac{Z_{0e}}{Z_{0o}}\right) - \tan^2\varphi\right]}{\left[\left(\dfrac{Z_{0e}}{Z_{0o}}\right) + \tan^2\varphi\right]} \tag{3.1}$$

From equation (3.1) the dispersive phase responses can be shown in Figure 3.2(b). Figure 3.2(b) indicates that, as two lines couple to each other (the coupling increases), the transmission phase ψ is reduced and, equivalently, the phase velocity is speeded up for $\psi < 180^o$. The frequencies around $\psi = 90^o$ have largest accelerating ratio.

Now, let us go back to the meandered parallel-coupled line in Figure 3.1. When the meandered coupled line is excited with even-mode, it can be equivalent to a single line Schiffman section because the even-mode modal current distribution of coupled line is similar to that of single line. Therefore, the even-mode phase velocity is accelerated when even-mode transmission phase $\theta_e < 180^o$. Therefore, the modal phase velocities can be equal at desired frequency with proper meandering.
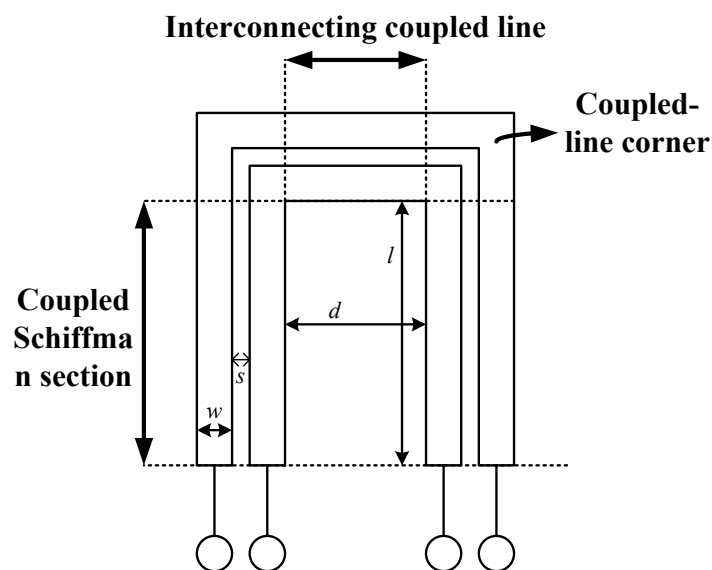
Figure 3.1   A standard meandered parallel coupled line.
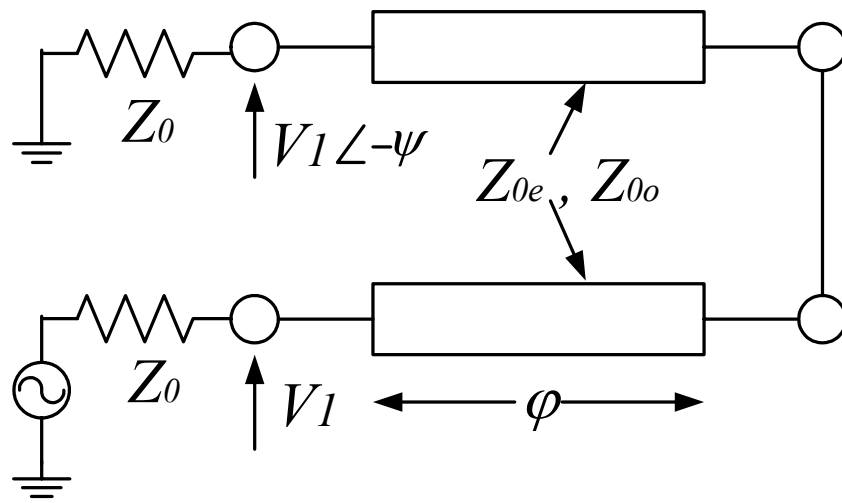
(a)
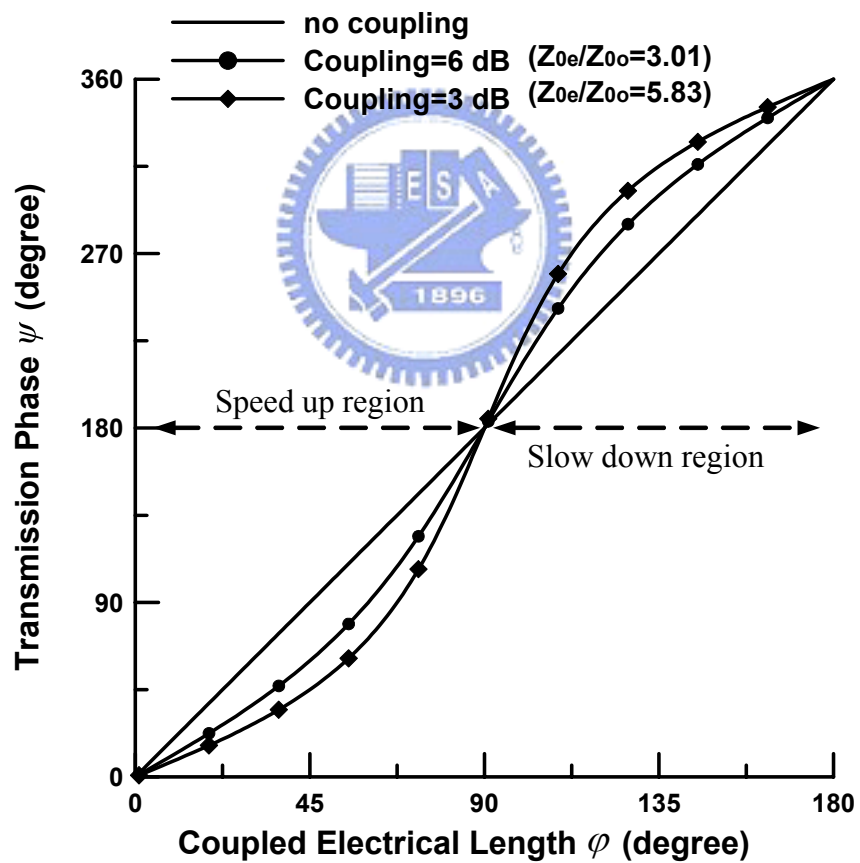
(b)

Figure 3.2   Schiffman section. (a) The schematic representation. (b) The dispersive phase responses.

A standard meandered parallel-coupled line is shown in Figure 3.1, which comprises an interconnecting coupled line, a coupled-Schiffman section, and two coupled-line corners. All circuit dimensions of the meandered parallel-coupled line are shown in Figure 3.1, where w is the line width, s is the line spacing, l is the coupled-Schiffman section length, d is the interconnecting coupled line length which is also called the meandered distance. The Z_{0e} and Z_{0o} of the meandered parallel-coupled line are different from those of the conventional parallel-coupled line. Figure 3.3 shows the variations of Z_{0e} and Z_{0o} of a meandered parallel-coupled line with different meandered distance. The curves shown in Figure 3.3 (a) corresponds to a meandered parallel-coupled line with w=20 mils, s=10 mils, L=600mils (capital L represents the total line length), and 50mil-thick Rogers RT6010 (ε_r=10.2) substrate. From Figure 3.3 (a), it can be observed that the Z_{0e} drastically reduces as the meandered distance decreases. And Z_{0o} just reduces a little. In order to see detail, we use 3D-Electroamagnetic (EM) simulator, High Frequency Structure Simulator (HFSS), to analysis the 3D structure that is shown in Figure 3.4. Figure 3.5 (a) points out that as the two coupled lines are excited in even mode, there are strong fields in the meandering region. That makes the total even-mode capacitance C_e drastically increases, and according to equation (2.7a), Z_{0e} reduces drastically. On the other hand, Figure 3.5 (b) indicates as the two coupled lines are excited in odd mode, there are still some weak fields in the meandering region, but the field strength is not as strong as the fields between the two main coupled lines. Therefore, odd-mode capacitance C_o only slightly increases, and Z_{0o} reduces slightly. In addition, characteristics of a meandered parallel-coupled line with a 20mil-thick Rogers RO4003 (ε_r=3.38) substrate, and physical parameter of w=10, s=4, and L=980 mils is shown in Figure 3.3 (b). The behaviors are similar to that of Figure 3.3 (a).

The θ_e and θ_o of the meandered parallel-coupled line are also different to those of the conventional parallel-coupled line. Figure 3.6 (a) and (b) depict the θ_e and θ_o of the meandered parallel-coupled lines with identical physical parameters as Figure 3.3 (a) and (b). Figure 3.6 indicates that the θ_e drastically reduces as d decreases. However, θ_o just has a little reduction. The main reason is the field distribution of the meandered parallel-coupled line is the similar to that of Schiffman section as the coupled line is excited by even mode. Therefore, the meandering induces dispersive effect and effectively speeds the V^e_p up. On the other hand, however, the field distribution of the odd-mode excitation is not similar to Schiffman, so there is no obvious speeding-up effect for V^o_p.

(a)

(b)

Figure 3.3   The even- and the odd-mode characteristic impedances with different
normalized meandered distance on (a) a 50mil-thick Rogers RT6010 substrate and (b)
a 20mil-thick Rogers RO4003 substrate.
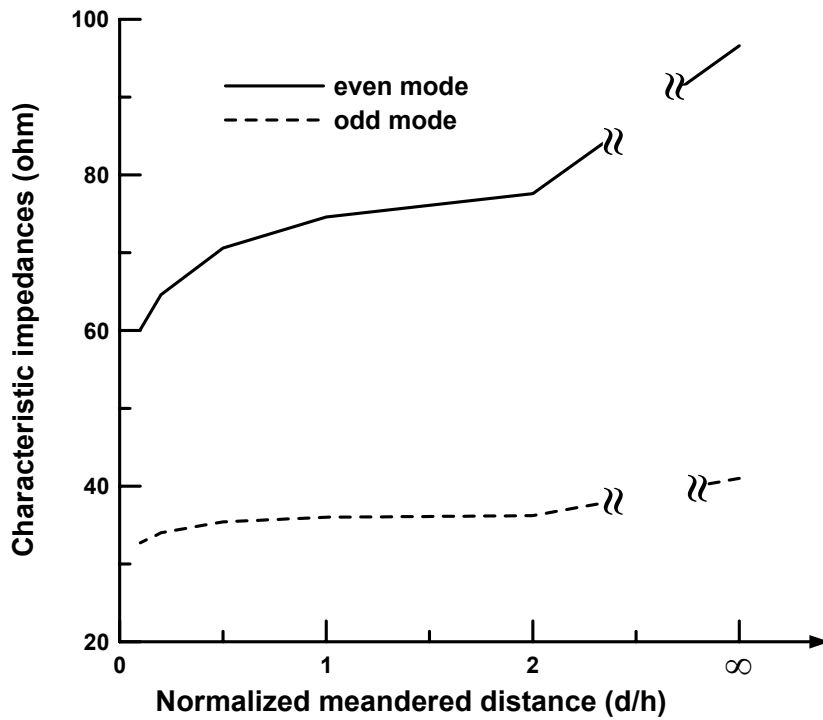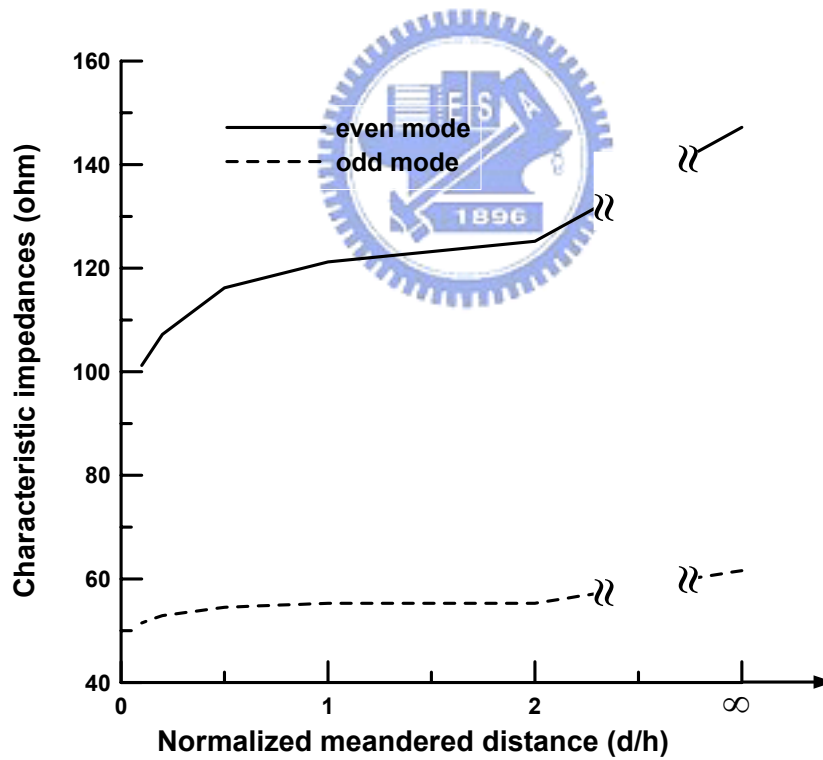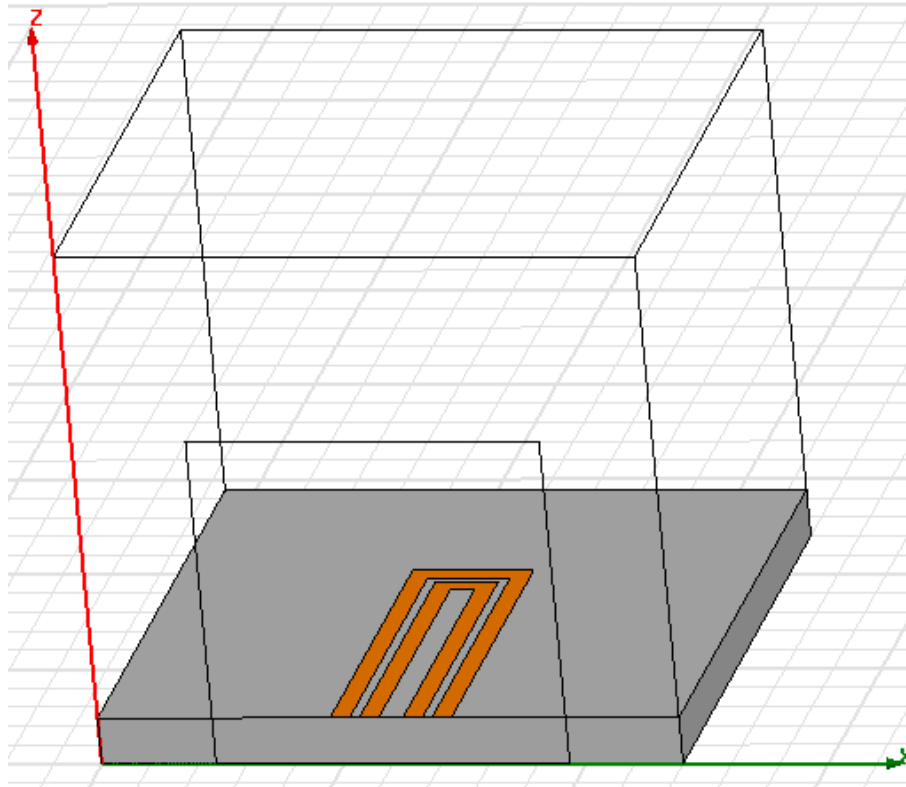
Figure 3.4   A standard meandered parallel coupled line in HFSS.
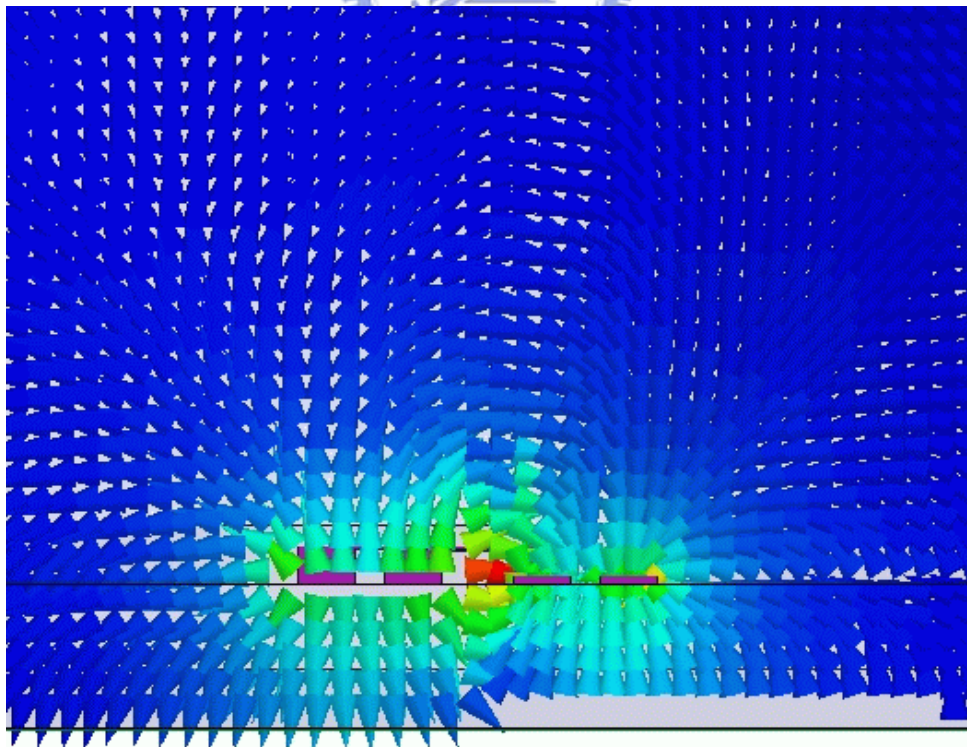
(a)
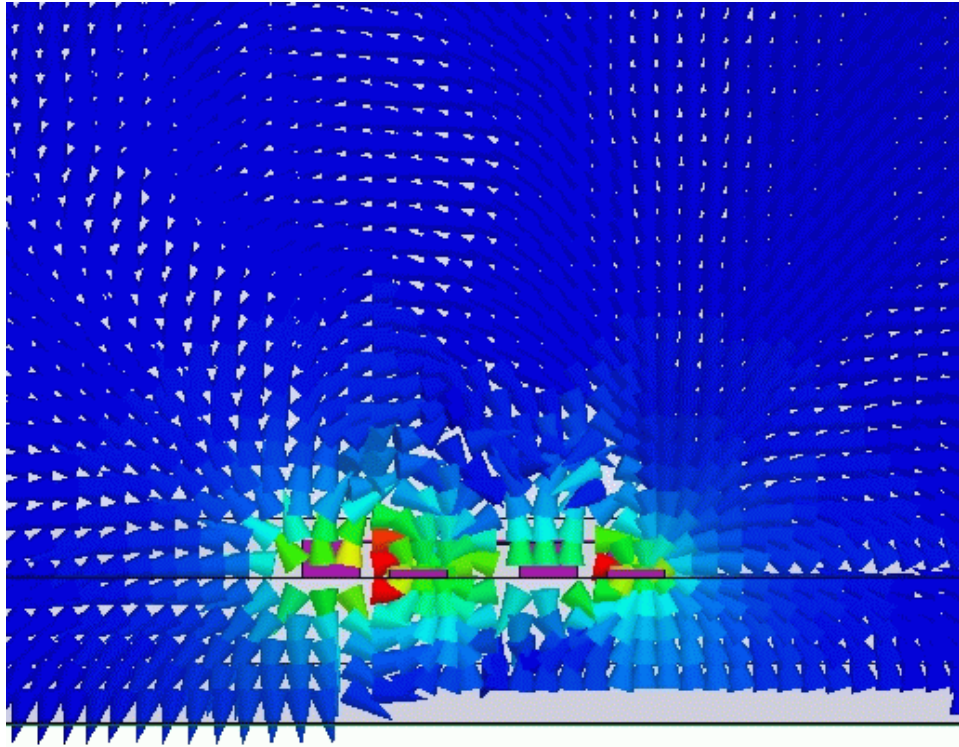
(b)

Figure 3.5   (a) The even- and (b) the odd-mode electrical fields in the cross-section.
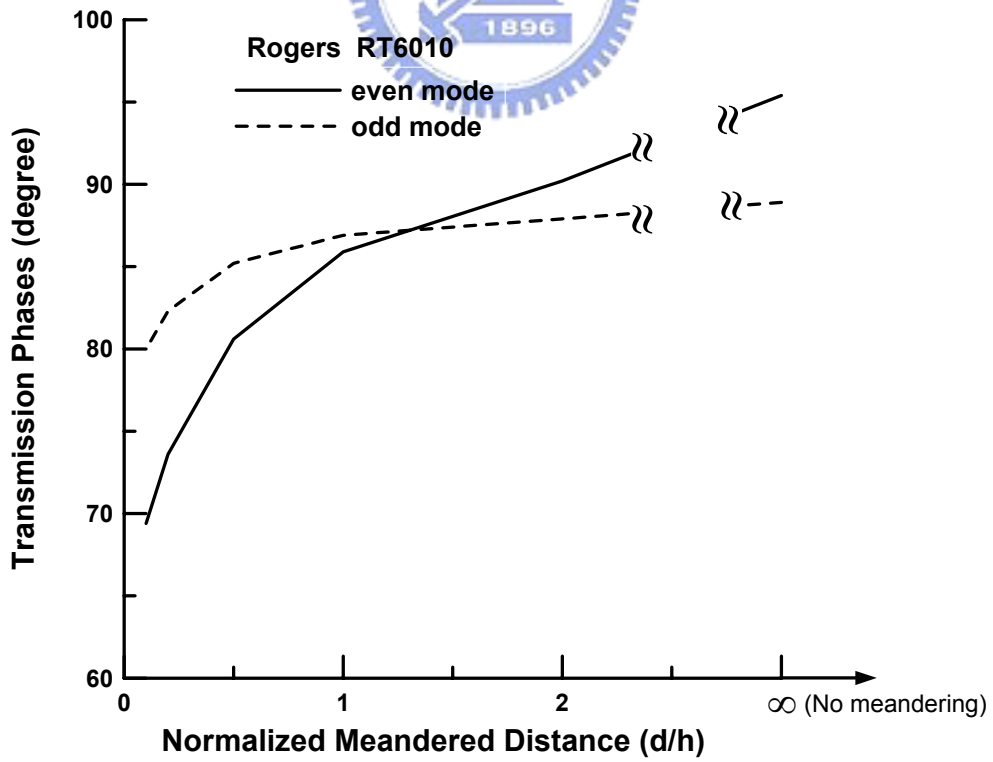
(a)
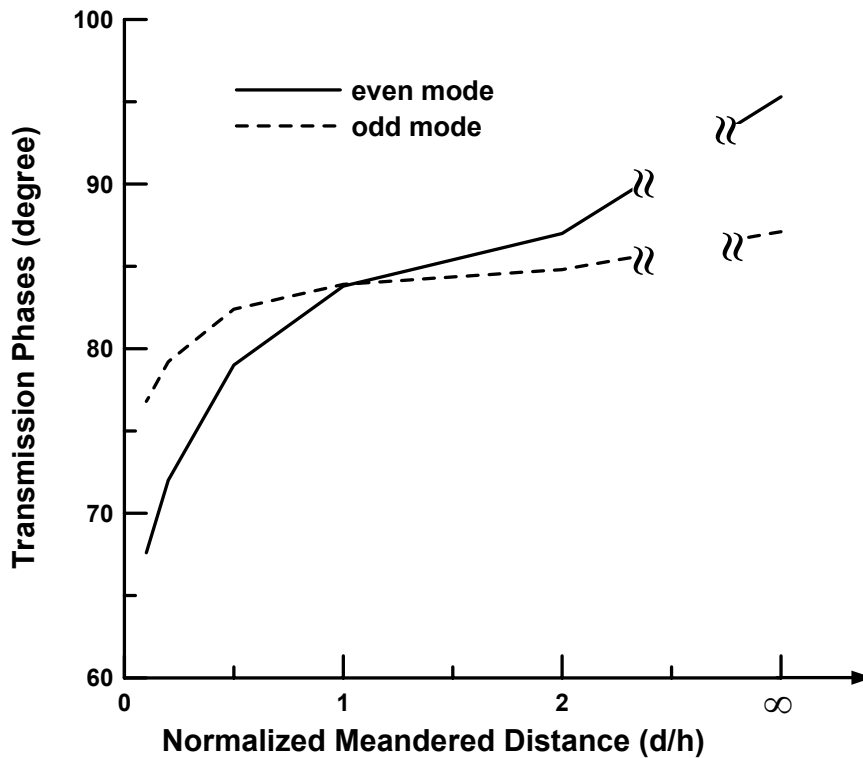
(b)

Figure 3.6 The even- and the odd-mode transmission phases (at 2 GHz) with different normalized meandered distance on (a) a 50mil-thick Rogers RT6010 substrate and (b) a 20mil-thick Rogers RO4003 substrate.

3.2 Synthesis of meandered parallel-coupled line

We hope that we can proper synthesis the physical dimensions of the meandered parallel-coupled line for various applications. However, there are no exact analysis or synthesis equations for meandered parallel-coupled line so that the circuit simulator such as Agilent ADS or AWR Microwave office is needed to analyze the behaviors of meandered parallel-coupled line. This section will describe how to use the circuit simulator to synthesize the exact physical dimensions of meandered parallel-coupled line according to the desired electrical parameters.

A standard meandered parallel-coupled line is shown in Figure 3.1, which comprises an interconnecting coupled line, a coupled-Schiffman section, and two coupled-line corners. The interconnecting coupled line uses the standard microstrip coupled line model in circuit simulator. The coupled-Schiffman section and the coupled-line corners are modeled in most of circuit simulators based on look up table of EM results. Using circuit simulator can quickly extract optimal dimensions of *w*, *s*,

l, and *d* in Figure 3.1. These dimensions have different weightings for coupler's modal characteristic impedances and modal transmission phases. In order to obtain desired coupling, the goal of the even- and the odd-mode characteristic impedance should be properly chosen respectively. Because the dimensions of *w* and *s* have larger weightings than *l* and *d* for the modal characteristic impedances of coupler, we optimize *w* and *s* in circuit simulator to obtain the desired modal characteristic impedances at desired frequency. Return loss is the criteria to observe whether the modal characteristic impedances to be fitted or not. On the other hand, in order to make the center frequency to locate at desired frequency, $\theta = 90^o$ (the average of modal transmission phases) is the criteria at desired center frequency. θ_e and θ_o should be equal at certain frequency where we want to get a good isolation. The dimensions *d* and *l* have larger weightings than *w* and *s* for the modal transmission phases of meandered section. The desired modal transmission phases can be obtained by adjusting *d* and *l*. However, because the modal characteristic impedances and modal transmission phases affect each other during adjusting process, iteration process is needed. We use the physical dimensions of conventional microstrip parallel coupler with the desired electrical parameters to be the initial guess in optimized procedures. Empirically, after several iteration cycles, the exact physical dimensions of meandered parallel-coupled line with desired electrical parameters can be obtained.

3.3 Coupler with ultra high directivity within a narrow band

According to the description in section 3.1, the coupled Schiffman section, a main part of meandered parallel-coupled line, can equivalently speed up the even-mode phase velocity. The scheme can be used to produce an intersection of θ_e and θ_o at any frequency point, and get an ultra high directivity at that frequency. This section will design a 10-dB coupler with ultra high directivity at 2.4 GHz based on single-section meandered parallel-coupled line, as shown in Figure 3.1, and fabricate it on an 50mil-thick Rogers RT6010 substrate with dielectric constant of 10.2.

From the specifications described above, the proper electrical parameters are Z_{0e} =69.4 ohm and Z_{0o} =36 ohm respectively. The physical dimensions of the coupler can be obtained initially by a circuit simulator. Both the weightings of physical dimensions for various electrical parameters and the iteration procedures are described in detail in section 3.2. Once obtaining these physical dimensions form the circuit simulator, the EM simulator such as Sonnet is used to do the fine tuning for getting the optimum performance. Finally, the optimum value of *w*=27 mils, *s*=12 mils, *l*=189 mils, *d*=30 mils is obtained by EM simulator. The modal transmission phases are shown in Figure 3.7. It can be found in Figure 3.7 that the even- and the

odd-mode transmission phases intersect at 2.4 GHz where the desired center frequency locates. The simulated and measured return losses are shown in Figure 3.8. Since a single-section meandered parallel-coupled line has an asymmetric layout between input and coupled port, the return loss data are took from the two ports. The simulated and measured return loss data agree well, and all show better than 20 dB return loss up to 2.6 GHz.

Figure 3.9 shows the simulated and measured coupling responses. We can observe the simulated and measured couplings are -12.4 dB and -12.3 dB at 2.4 GHz, respectively. The curves are matched well.

The simulated and measured isolations are -76 and -67 dB at center frequency, respectively, as shown in Figure 3.10. The measured response matches well with the simulated one, and both have a more than 40 dB improvement comparing to that of conventional coupler.

Figure 3.11 shows the simulated and measured directivities. The simulated and measured directivities are 64.6 and 54.7 dB at center frequency, respectively, and they match well around center frequency. Figure 3.12 (a) and (b) show the layout and photograph of proposed coupler.
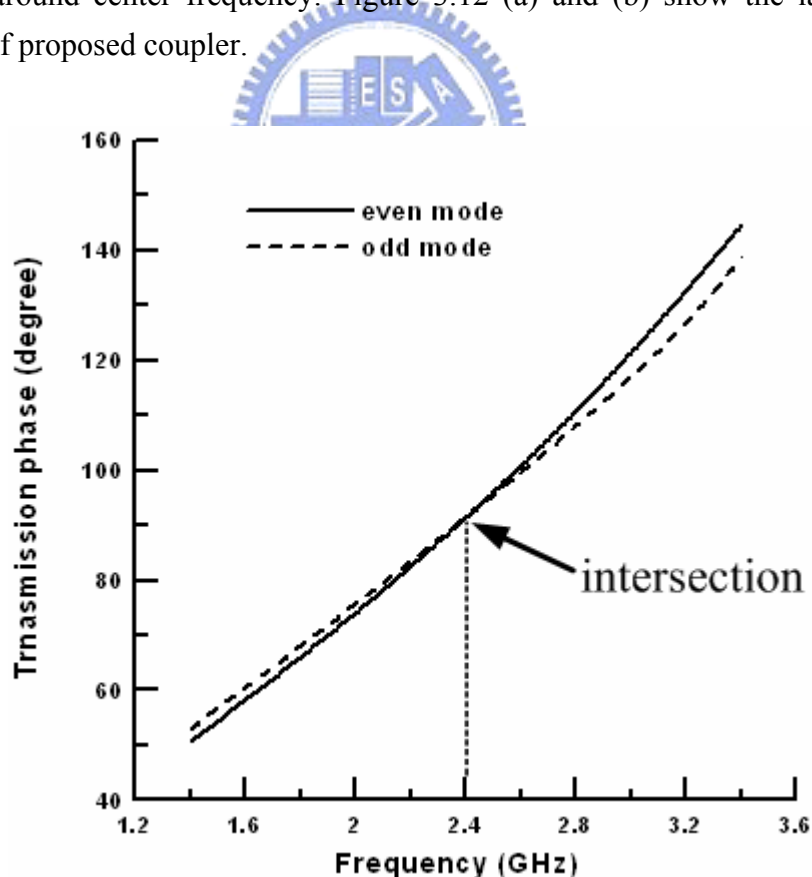
Figure 3.7   The modal transmission phases of single section meandered parallel-coupled line.

Figure 3.8   The simulated and measured return losses of the single section meandered parallel-coupled line.
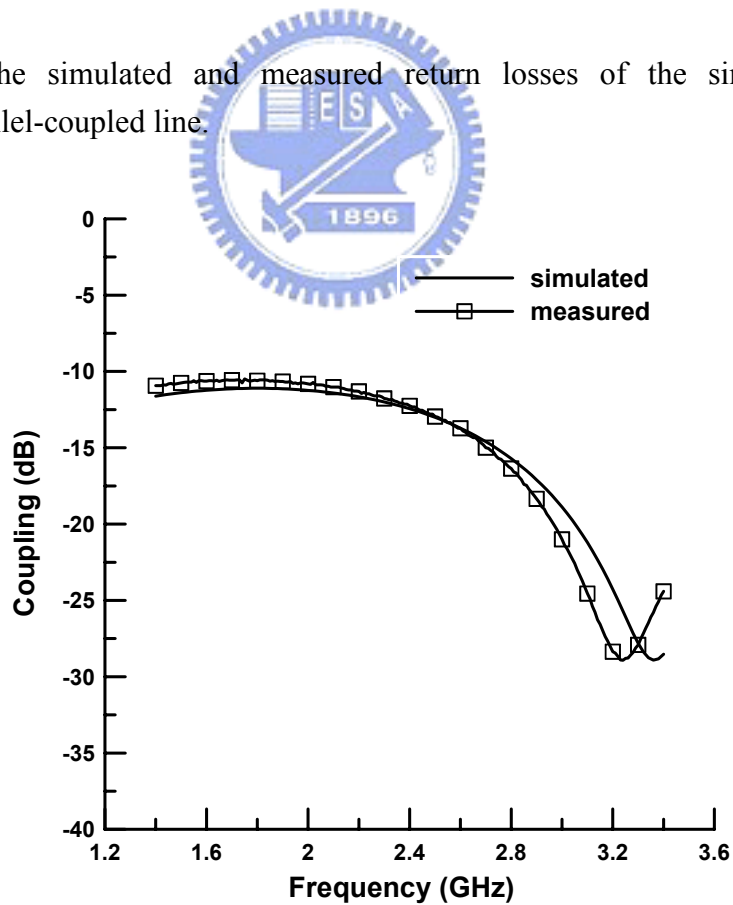
Figure 3.9   The simulated and measured couplings of the single section meandered parallel-coupled line.

31

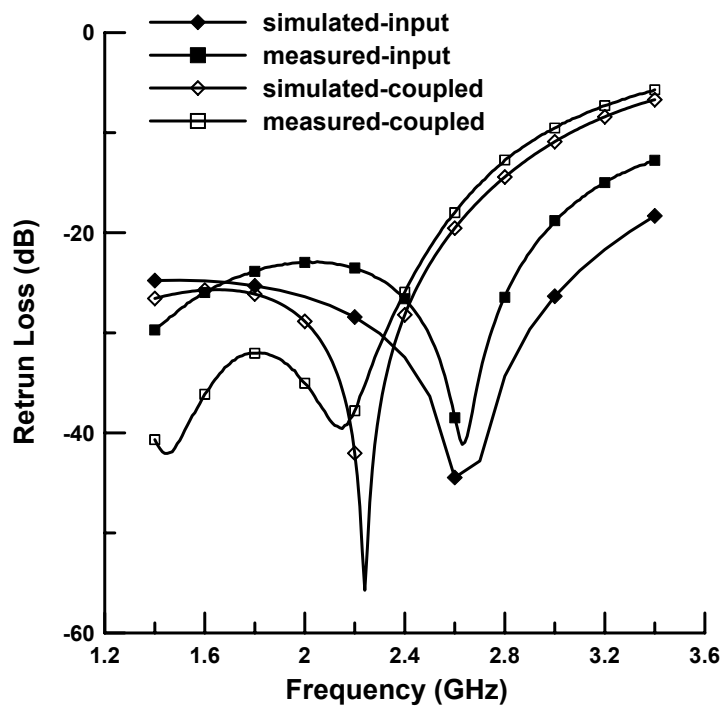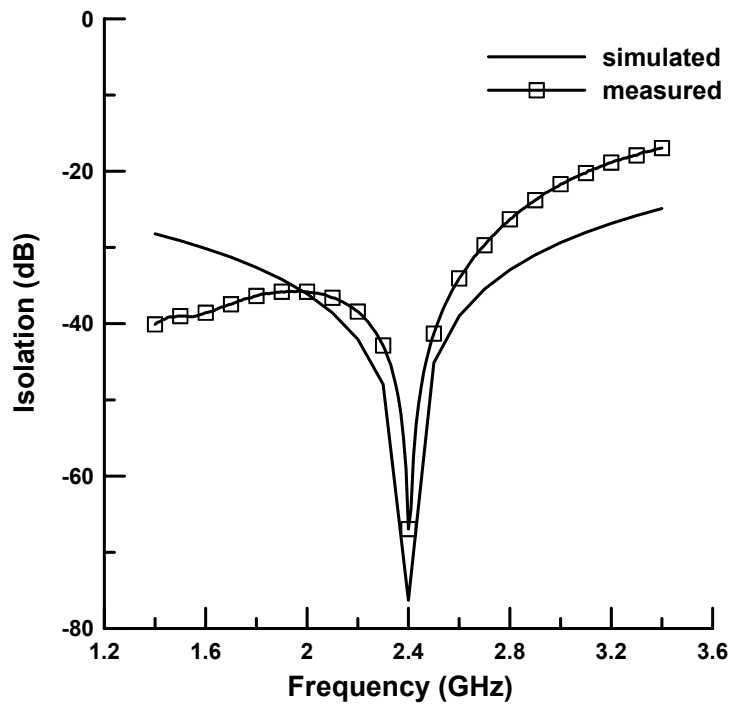Figure 3.10   The simulated and measured isolations of the single section meandered parallel-coupled line.
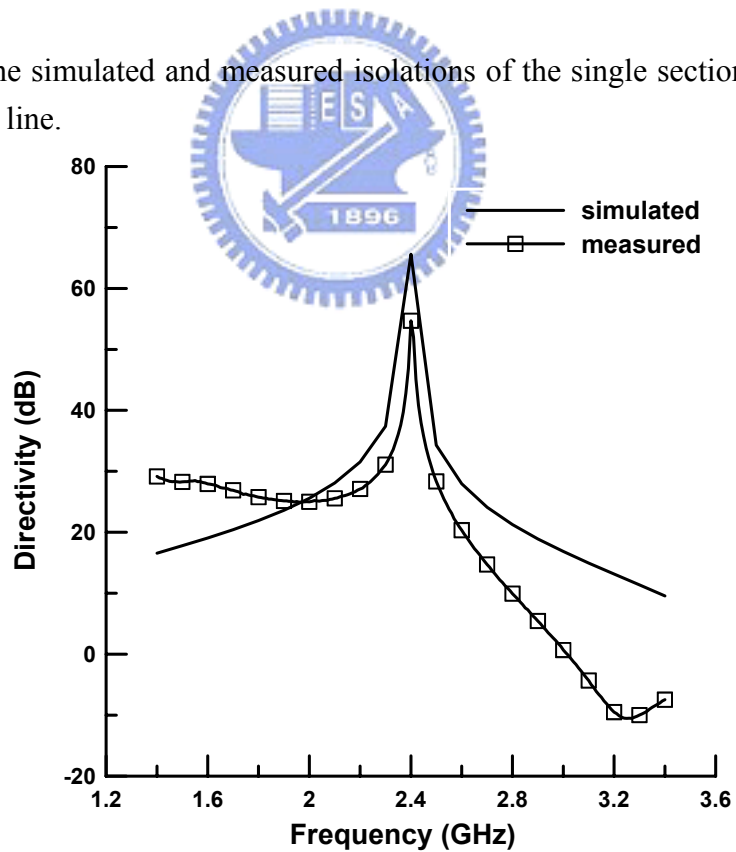
Figure 3.11   The simulated and measured directivities of the single section meandered parallel-coupled line.

32

From these results, we give some conclusions. First, it can be observed that the return losses in Figure 3.8 drastically get worse when the frequency is higher than 3 GHz. The reason is that the Z_{0e} of single section meandered parallel-coupled line varies as frequency when the frequency is higher than about 1.5 times of center frequency. Figure 3.13 (a) shows a simplified equivalent circuit of Figure 3.1. Here, the coupled-line corner and interconnect coupled line are absorbed into coupled Schiffman section. The various dimensions of this single section meandered parallel-coupled line are shown in Figure 3.13 (a). With even mode excitation, Figure 3.13 (a) can be simplified to Figure 3.13 (b), a meandered single microstrip line with $2w+s$ of line width. The electrical parameters are Z_{0e} =48.8 ohm, Z_{0o} =32.8 ohm, $\varepsilon^{e}_{r\_eff}$ =7.88, and $\varepsilon^{o}_{r\_eff}$ =6.07 for the circuit in Figure 3.13 (b). Refer to [24], the image impedance Z_i of the structure shown in Figure 3.13 (b) is the square root of Z_{0e} by Z_{0o}. Therefore, if we set the port impedance to be the theoretical Z_i, 40 ohm, we should get a perfect port matching. But it isn't correct for our case. Because the theory of [24] is based on TEM mode, however, the $\varepsilon^{e}_{r\_eff}$, and $\varepsilon^{o}_{r\_eff}$ in the structure of Figure 3.13 (b) are not equal. Thus, it is not a pure TEM mode. The obtained return losses shown in Figure 3.14 (a) are not a perfect port matching. And the return losses are worse than -20 dB as the frequency is higher than 2.5 GHz. Here, we tune the Z_i to be 34.7 ohm to obtain a wider port matching bandwidth. The results are shown in Figure 3.14 (b). It indicates the return losses are better than -20 dB as the frequency is lower than 3.5 GHz. We can get the desired Z_i by this way. Since Z_i is equivalent to the shunt circuit of the two coupled lines with characteristic impedance Z_{0e}, the Z_{0e} is two times of Z_i, 69.4 ohm, the value that we want. This value is useful when frequency is lower than 3.5 GHz. When frequency is higher than 3.5 GHz, the Z_{0e} still drastically varies as frequency due to the inherent characteristic of the meandered coupled line. Fortunately, the Z_{0o} of single section meandered parallel-coupled line is almost a constant of frequency, just likes the Z_{0o} in conventional parallel coupler. Therefore, the main reason that makes the return loss of the proposed coupler to get worse is the non-constant characteristic of Z_{0e}.

Second, since the proposed structure in Figure 3.1 is an asymmetric structure, mode coupling would be happen. That means the even and odd mode will simultaneously exist whether even or odd mode is excited. In this case, the even- and odd-mode scattering parameters can be calculated from the normal-mode scattering parameters obtained by EM simulation and then the mode coupling can be observed. The magnitude of the mode coupling can be as high as one-third that of excitation mode (about -10dB of mode conversion). Fortunately, the analysis based on even- and odd-mode analysis is still useful and it will be proved by several design examples.

In addition, the right-angle corner in Figure 3.1 would produce radiation loss or surface wave loss. As shown in Figure 3.15, the sum of square of normal scattering parameters is less than unity as frequency goes high. That implies the radiation loss or surface wave loss exists and results in extra loss.

Finally, Figure 3.2(b) indicates that the θ_e versus frequency will be a curve due to the dispersion (or speeding-up) effect. And we know that the θ_o versus frequency is almost linear for a meandered parallel-coupled line. It is known that every phase versus frequency curve of a quasi-TEM coupled line started from the origin of the coordinate. Unfortunately, a curved line like Figure 3.2(b) and a linear straight line can only have one intersection point other than zero frequency. There is only one intersection at center frequency as shown in Figure 3.7. This means that this coupler can only have one ultra-high directivity frequency point where it is chosen to be the certain frequency.
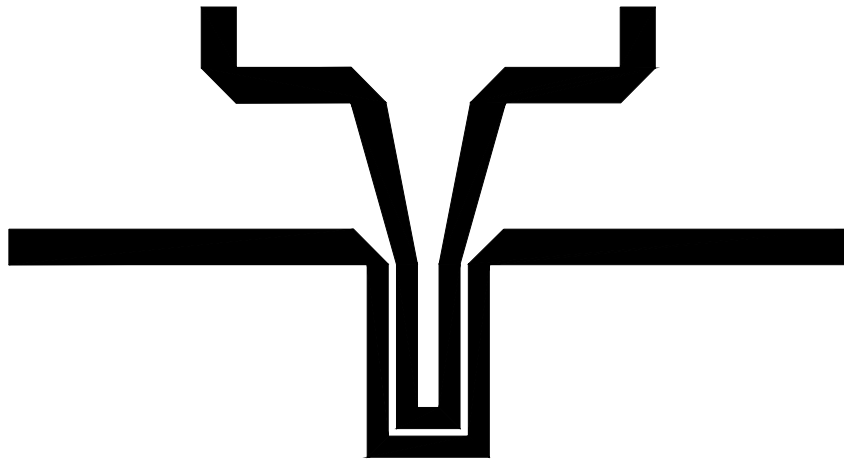
(a)
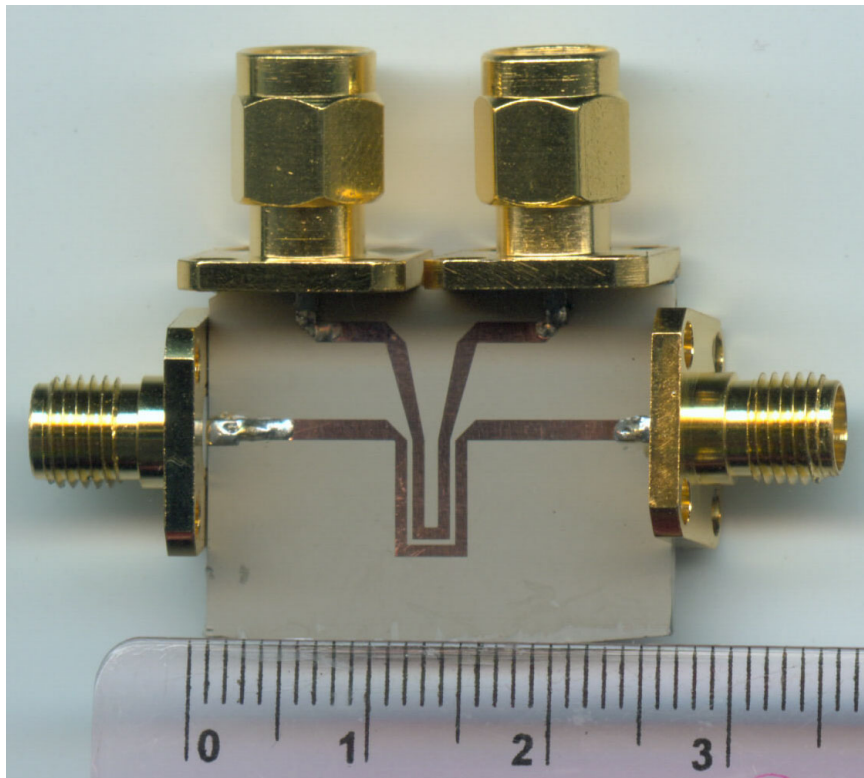
(b)

Figure 3.12   The (a) layout and (b) photograph of the coupler with ultra high directivity.
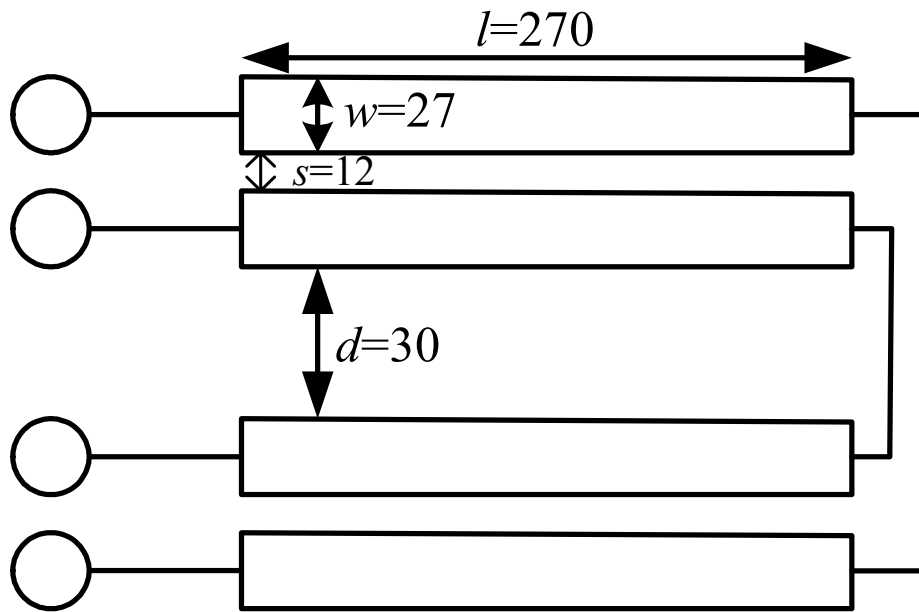
(a)
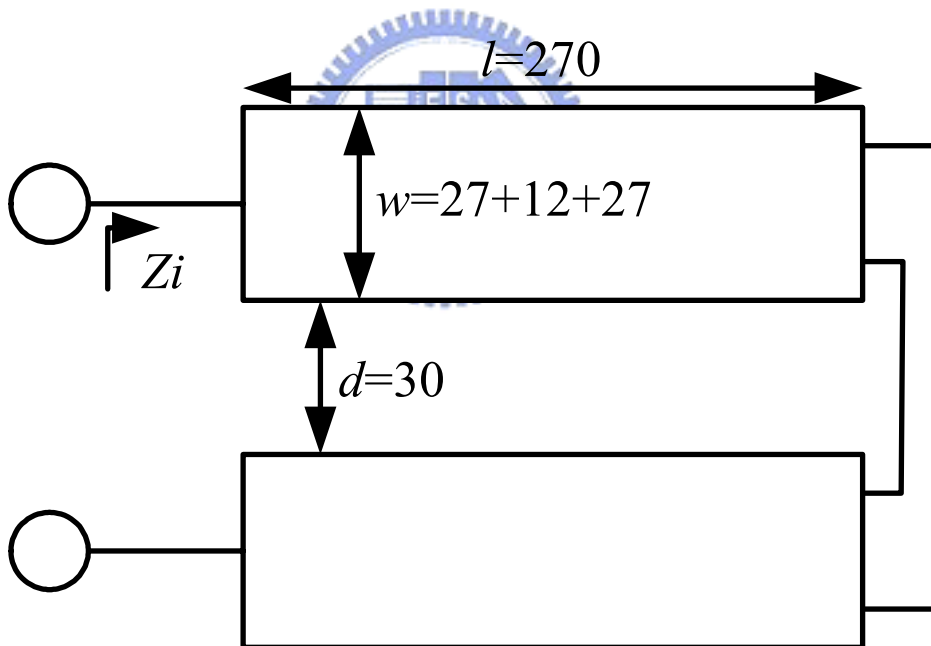
(b)

Figure 3.13   (a) The simplified equivalent circuit of Figure 3.1 (b) the simplified equivalent of (a) in even mode excitation. (Unit: mils)

(a)
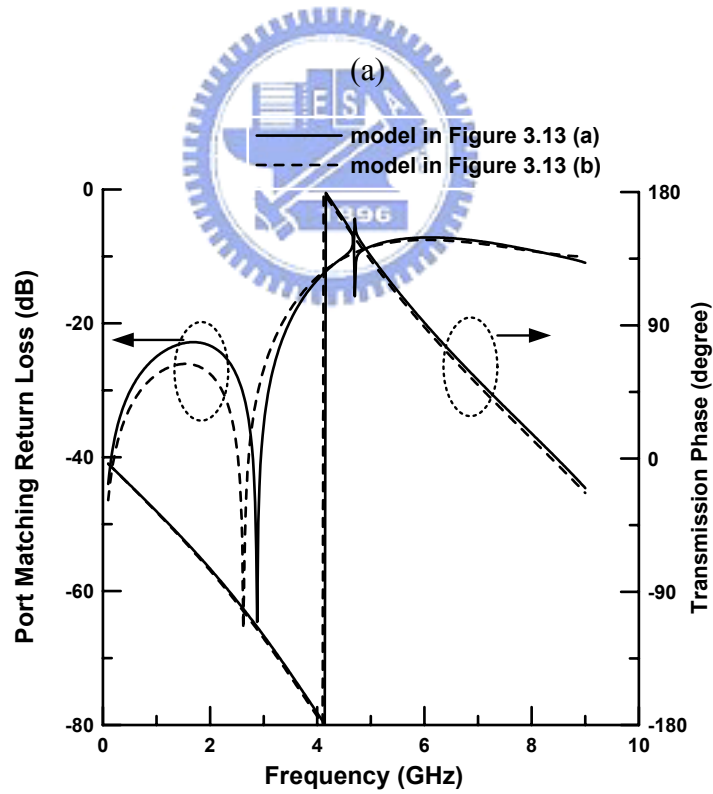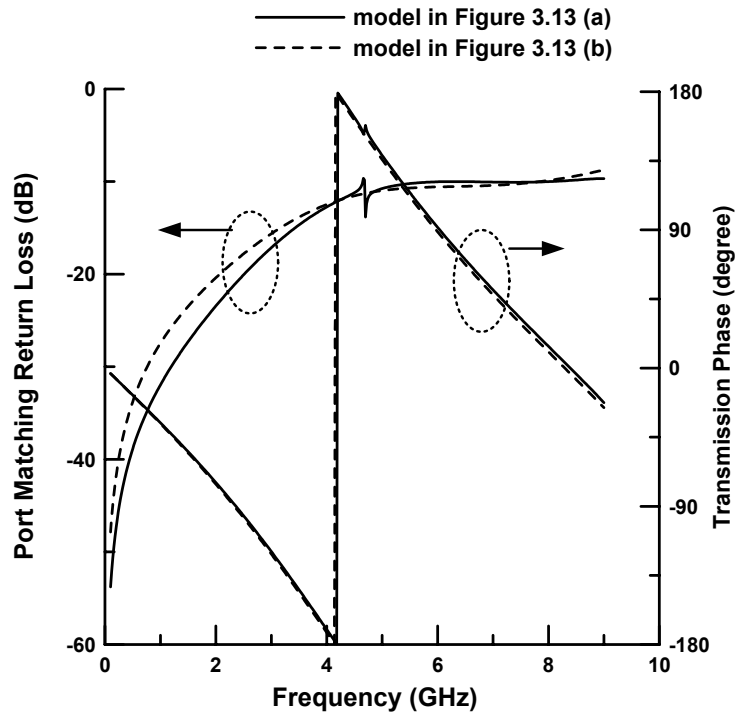
(b)

Figure 3.14   The port matching responses and transmission phases of the equivalent circuits in Figure 3.13 with (a) theoretical Z_i and (b) tuned Z_i.
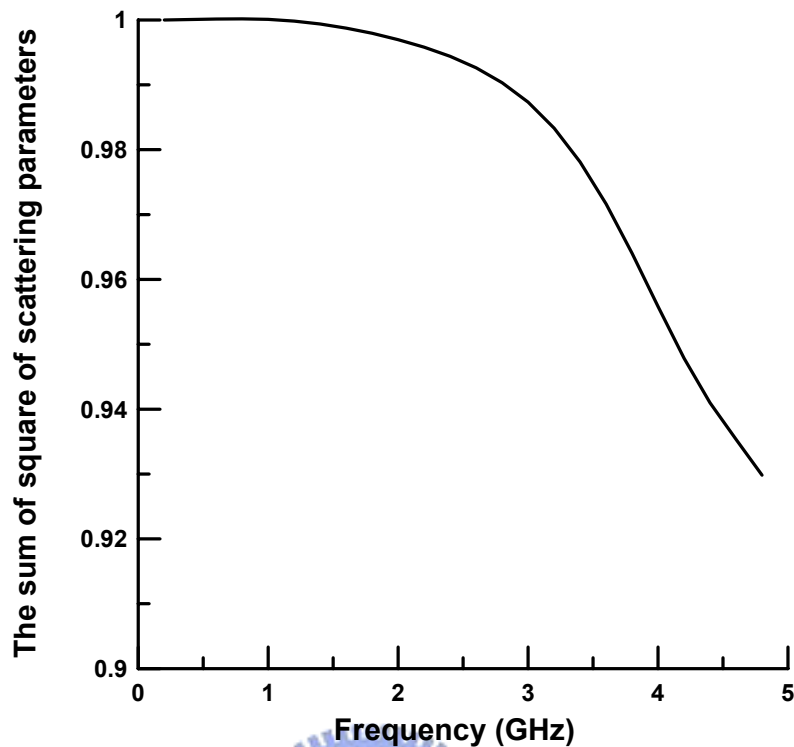
Figure 3.15   The sum of square of scattering parameters versus frequency.

3.4 Coupler with high directivity over broad bandwidth

Last section described the single-section meandered parallel-coupled line can only get ultra-high directivity around a narrow frequency band. In order to make the high directivity bandwidth wider like a pure TEM coupled line, we propose a multisection meandered parallel coupler, as shown in Figure 3.16(a). Cascading of several identical unit-meandered-sections forms the proposed coupler. The unit-meandered-section is shown in Figure 3.16(b). Figure 3.17 shows the transmission phase of conventional and proposed coupler. Here, we pay our attention to the bandwidth between 0 and $2f_o$, which is the main operation bandwidth of a coupler. In Figure 3.17, the modal transmission phases of conventional parallel-coupled-line coupler are shown as solid lines. In addition, in order to explain conveniently, we neglect the tiny variation of the odd-mode transmission phase caused by meandering. The even-mode transmission phases of whole coupler with one, two and five meandered sections are shown in Figure 3.17. In Figure 3.17, the θ_e with one meandered section is a curve, and as the number of the meandered section increases, the even-mode transmission phase approaches a straight line. The

dispersion curve of θ_e approaches a straight line because only a small portion of θ_e curve is taken as the number of section increases. Therefore, θ_e can approach θ_o over a very wide bandwidth. Based on the scheme, a microstrip coupler with nearly ideal TEM coupler performance can be achieved over the entire coupler bandwidth.

(a)

(b)
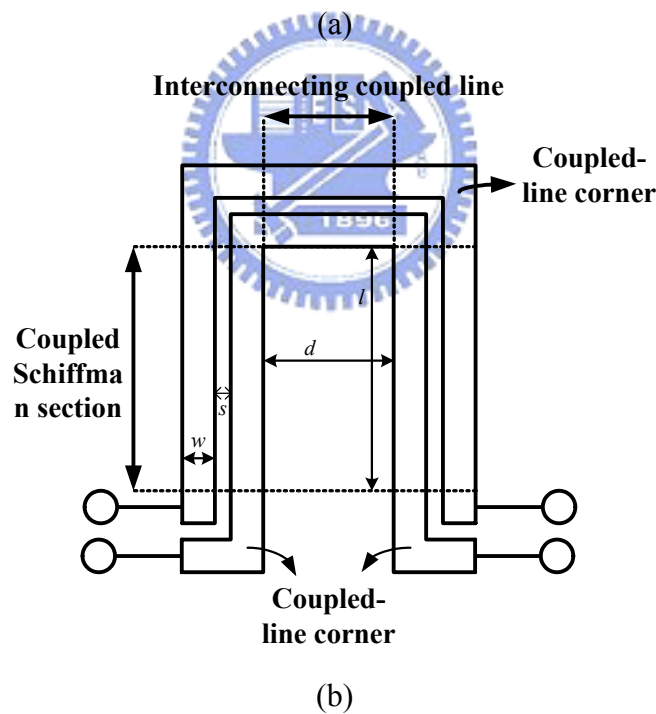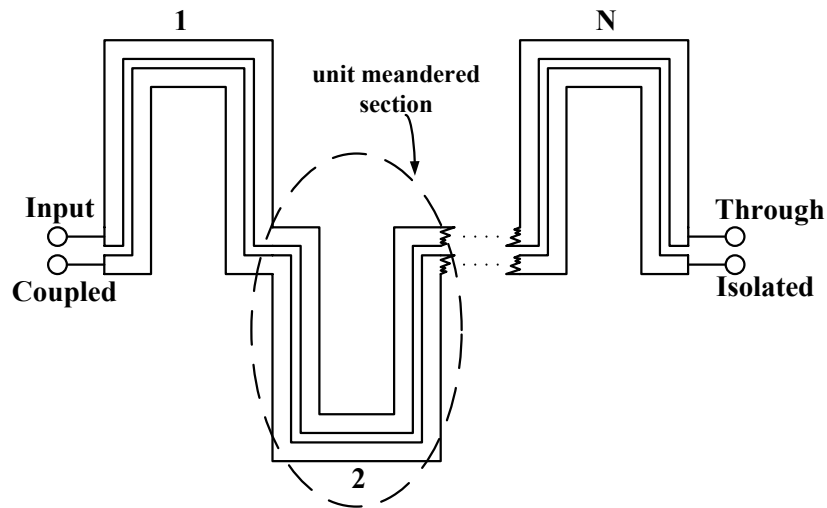
Figure 3.16   (a) The multisection meandered parallel-coupled line. (b) The unit-meandered-section.

Because an ideal TEM coupler repeats its response every $2f_o$, the target of the design is to equalize θ_e and θ_o within $2f_o$ (i.e. within the first period of response). We take a 20-dB coupler at 1GHz as a design example. The circuit is fabricated on an 8mil-thick Rogers RO4003 substrate with dielectric constant of 3.38. In order to

achieve the design goal, we implement the coupler with five unit meandered sections. As shown in Figure 3.16 (b), the unit meandered section comprises an interconnecting coupled line, a coupled-Schiffman section, and four coupled-line corners. The synthesis procedures have been described in section 3.2, the only difference with respect to the circuit described in section 3.2 is two extra coupled line corners. Here, in order to obtain 20-dB coupling, the theoretical values of Z_{0e} and Z_{0o} should be 55.3 and 45.2 ohm respectively. On the other hand, in order to make the center frequency to locate at 1 GHz, the θ_o should be 18° (90° divide by 5) at 1GHz and θ_e must be as close to θ_o as possible. After obtaining the appropriate dimensions of unit meandered section, the coupler design is finished by cascading five identical meandered sections. Finally, the whole coupler is fine-tuned by EM simulator Sonnet. The physical layout dimensions of unit meandered section are as follows that w, s, l, d are 16.5, 7.5, 119.5, 2.5 mils, respectively.

The EM-simulated and measured coupling and return loss are shown in Figure 3.18. Good match are observed. The simulated and measured couplings are -20.6 and -20 dB, respectively. Both simulated and measured isolations have excellent response of below –50dB from 0 to 2GHz as shown in Figure 3.19. Also shown in Figure 3.19, the isolation of a conventional coupler with the same coupling is measured for comparison, and a significant improvement can be observed. Figure 3.20 is the layout of the proposed coupler. Figure 3.21 depicts the photograph of the proposed coupler and a conventional straight coupler to see the significant size reduction.
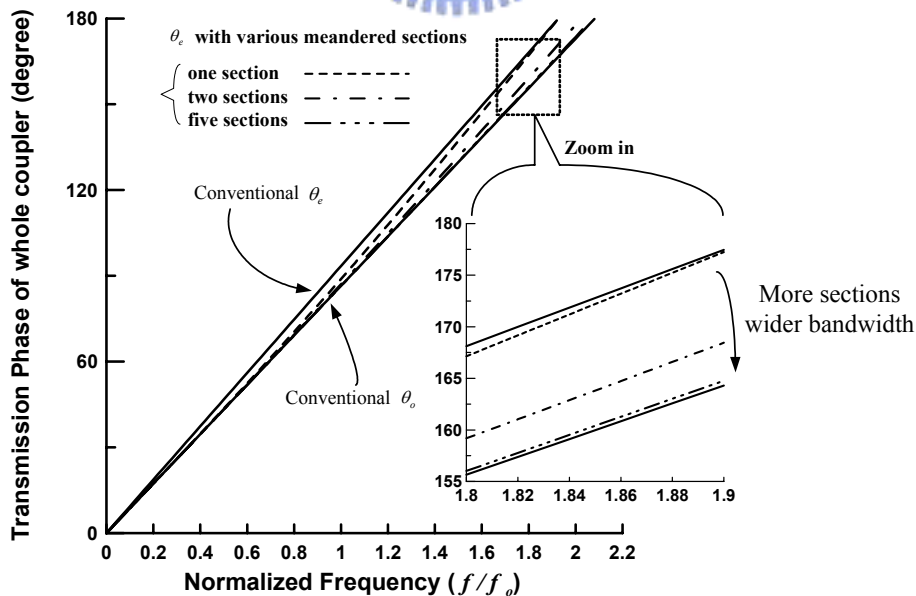
Figure 3.17   The modal transmission phases of conventional parallel-coupled-line coupler and the even-mode transmission phase with single, two, and five meandered sections.
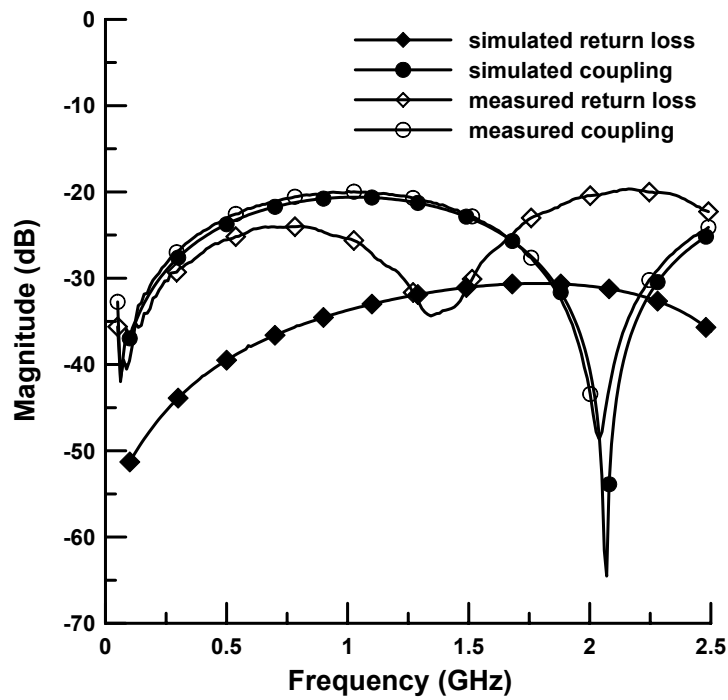
Figure 3.18   The simulated and measured return loss and coupling of the proposed coupler.
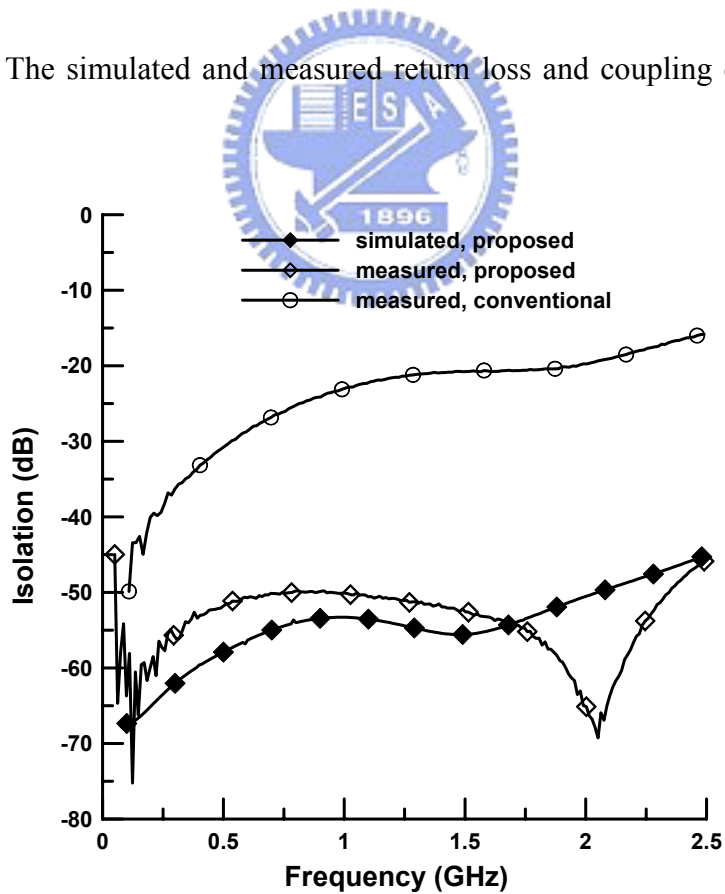
Figure 3.19   The simulated and measured isolation of the proposed coupler and measured isolation of a conventional coupler with the same specification.
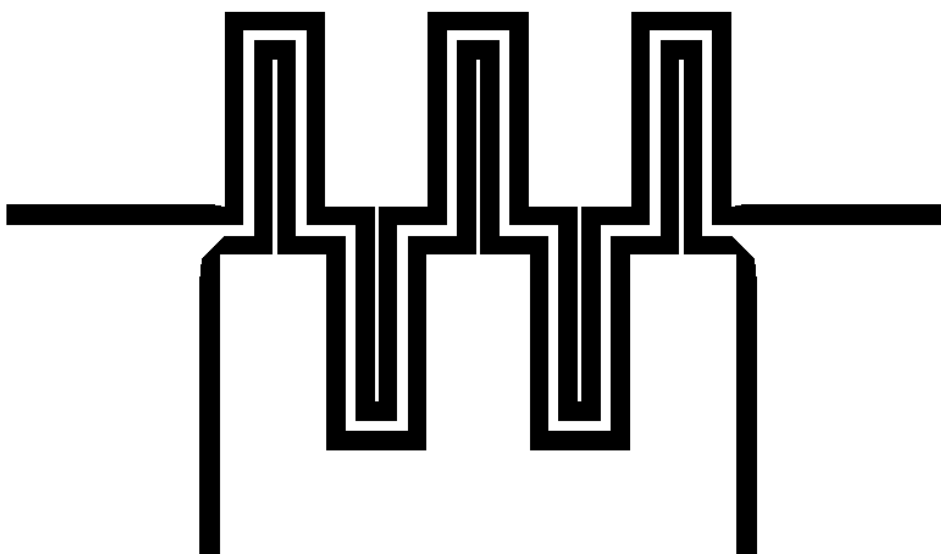
Figure 3.20   The layout of the proposed coupler.
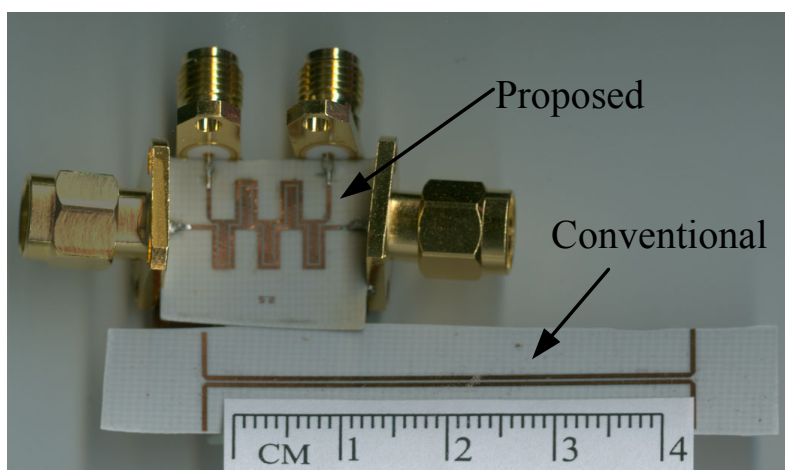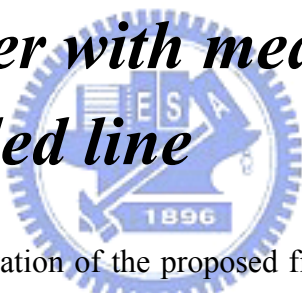
Figure 3.21   The circuit size comparison between proposed and conventional coupler.

Chapter 4

Analysis, design and realization of band pass filter with meandered parallel coupled line

In this chapter, the motivation of the proposed filter is from section 3.1 that the even-mode phase velocity can be speeded up by meandering a parallel-coupled line. In this chapter the same idea can be applied to a microstrip filter to improve its performances. As meandering a parallel-coupled filter properly, not only the filter's first spurious passband near $2f_o$ can be suppressed but also its size can be reduced drastically. And there is no precedent that a parallel-coupled filter can simultaneously suppress the spurious passband and greatly reduce its size. Furthermore, the proposed structure needs no additional circuit components or fabrication process such as capacitors or via holes so that low fabrication cost can be kept.

Each parallel-coupled section of a conventional parallel-coupled filter is meandered in the proposed filter. The new parallel-coupled section can be modeled as a meandered parallel-coupled line, and a commercial circuit simulator can analyze it. In this dissertation, the behaviors of the meandered parallel-coupled line are explained particularly. Systematic design procedures of the proposed filter are described in detail. Several meandered parallel-coupled microstrip filters are fabricated with various specifications, and the measured results match well with simulation.

4.1 Previous works for removing spurious passband

The microstrip parallel-coupled filter first proposed by Cohn in 1958 [25] has been widely used in many microwave and wireless communication systems. This type of filter is popular due to its planar structure, insensitive to fabrication tolerance, wide realizable bandwidth (from a few percent to more than 60 percent) [26-28], and simple synthesis procedures [29]. However, there are several disadvantages of the conventional microstrip parallel-coupled filter. One of the disadvantages is that the first spurious passband of this type of filter appears at twice of the basic passband frequency ($2f_o$). Therefore, the rejection of the upper stopband is worse than that of the lower stopband. Sometimes, the upper stopband rejection may be as bad as -10 dB, especially in case of wide bandwidth filters. Another disadvantage is the whole length of the filter is too long especially when the order of a filter becomes high. Both disadvantages greatly limit the application of this type of filter.

The reason for the first spurious passband is that the even-mode phase velocity is always slower than that of the odd-mode because of the inhomogeneous medium of microstrip structure. The unequal modal phase velocities at $2f_o$ cause the first spurious passband. There are two basic methods to equalize the modal transmission phase: providing different lengths for the even- and odd-mode, or equalizing the modal phase velocities. In [28] and [30], an over-coupled resonator is proposed to extend the electrical length of the odd-mode to compensate the difference in the phase velocities. The structure in [7] and [32] uses capacitors to slow down the odd mode phase velocity. The substrate suspension structures in [33] are substantially designed to speed up the even-mode phase velocity, and make the modal phase velocities equal. The wiggly-coupled microstrip filter in [34] is also effective in improving the rejection characteristics of the filter at $2f_o$. These published filters have some drawbacks. Firstly, all these filters in [7, 29-33] are too long due to their straight structure especially when the order of the filter becomes high. The filters in [7] and [32] need extra circuit components that cause higher material and assembly cost. The filter in [33] needs to suspended the substrate and a costly package is required. The filters in [30], [31], [33], and [34] are with complex design procedures.

An alternative method to eliminate spurious passband is to use a self-filtering resonator [35] where the resonator is formed by a high-low impedance lowpass filter. This kind of resonator is complex to layout as a parallel-coupled filter. Moreover, due to the limitation of the high-low impedance ratio of the resonator, the spurious passband suppression is usually limited unless a three dimensional structure is used.

Another method to improve a parallel-coupled filter's upper stopband

44

performance is to move the first spurious passband away from $2f_o$ [36], [37]. Usually using the step impedance resonator can shift the first higher order resonant frequency of a resonator. However, the step impedance method is to move, not to suppress, the first spurious band. If we want to move the first spurious passband to $3f_o$ a large impedance stepping ratio of the resonator is required and the layout of the filter becomes difficult.

4.2 The mechanism of modified MPCL to suppress spurious passband

The schematic of a parallel-coupled bandpass section is shown in Figure 4.1(a), and its equivalent circuit proposed by Matthaei [25] is shown in Figure 4.1(b). Where Z_{0e} and Z_{0o} are the even- and odd-mode characteristic impedances. The coupled electrical length θ, even-mode transmission phase θ_e, and odd-mode transmission phase θ_o are given by equation (2.14), (2,15a), and (2.15b), respectively. Here, the equivalent circuit in Figure 4.1(b) is based on TEM mode, and θ_e and θ_o are both equal to θ for all frequencies. From Figure 4.1(b) at $2f_o$, because $\theta_e = \theta_o = 180^o$, the series open stub will be open circuited at its input end. The transmission line between two series open stubs is now at its half wavelength resonant frequency where the first spurious passband locates. Since two series open stubs are open circuited at their ends, no energy can be coupled to the half-wave resonator and a stopband will be formed. Therefore, the ultimate target of spurious passband suppression is to achieve $\theta_e = \theta_o = 180^o$ at $2f_o$. Unfortunately, in microstrip structure, because the even-mode phase velocity of a microstrip coupled line is always slower than that of the odd-mode, θ_e is always larger than θ_o for all frequencies. Therefore, the spurious passband of a conventional microstrip parallel-coupled filter at $2f_o$ occurs.

$$Z_{0e}, Z_{0o}$$

$$\theta$$

(a)

(b)
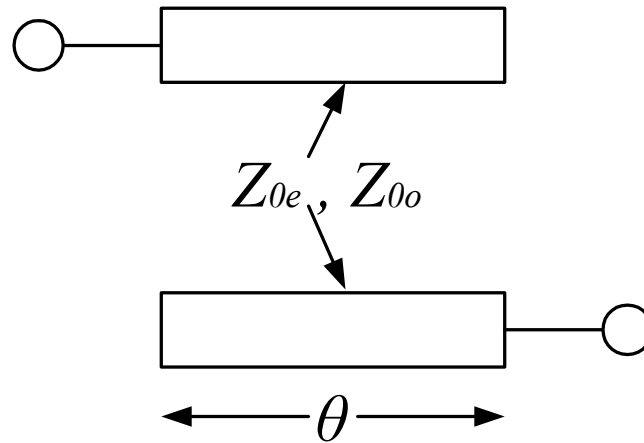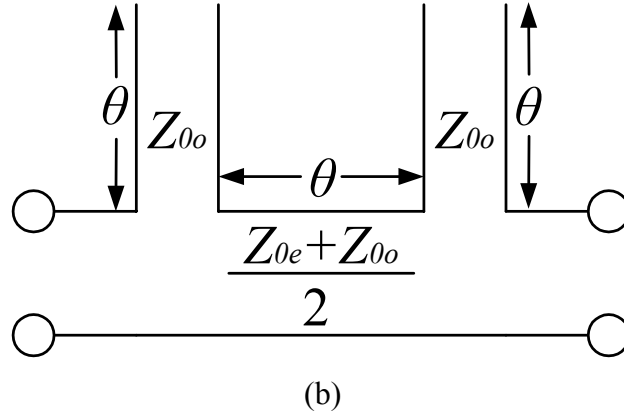
Figure 4.1   A TEM parallel-coupled bandpass section. (a) The schematic representation. (b) The equivalent circuit.

Figure 4.2(a) shows a conventional parallel-coupled line section. Figure 4.2(b) depicts the proposed meandered parallel-coupled line section, which is the basic building block of our parallel-coupled line filter. The coupled line in Figure 4.2(b) is the variation of Figure 4.2(a). All circuit dimensions of the meandered parallel coupled line are shown in Figure 4.2(b), where w is the line width, s is the line spacing, l is the coupled-Schiffman section length, d is the interconnecting coupled-line length which is also called the meandered distance, and b is the tail coupled-line length. The meandered parallel-coupled line section shown in Figure 4.2(b) has the advantage of reducing the circuit size and equalizing the modal transmission phases. The effects of equalizing the modal transmission phases are originated from the coupled-Schiffman section. As discussed in section 3.1, the coupled-Schiffman section speeds up the even-mode phase velocity. In addition, because the odd-mode current distribution cannot be approximated to that of the Schiffman section, the odd-mode phase velocity is not obviously increased as the even mode. By EM simulation, the odd-mode phase velocity is found to increase slightly.

In order to explain conveniently, in this section, we neglect the tiny variation of the odd-mode transmission phase caused by meandering. The main mechanism of the proposed structure is to speed up the even-mode phase velocity and to achieve the target of $\theta_e = \theta_o = 180^o$ at $2f_o$. Since odd-mode transmission phase θ_o is supposed to be not affected by meandering, the total length of the proposed meandered parallel coupled line equals to that of conventional coupled line and the total length L is chosen to be $\theta_o = 180^o$ at $2f_o$. θ_e and θ_o of a conventional coupled line are shown as the hollow-triangle dashed line and the hollow-square line in Figure 4.3 respectively. θ_o is

46

smaller than θ_e, and their difference is increased proportional to frequency. Now, if the coupled-line corners and interconnecting and tail coupled line are omitted, the even-mode phase velocity of a coupled-Schiffman section with length $L/2$ is decelerated at $2f_o$ as the hollow-circle curve shown in Figure 4.3. This is because the phase velocity accelerating region of a Schiffman section locates in the region of $\theta_e <$ 180° and the most effective accelerating region is θ_e closed to 90°. Therefore, in order to make the desired $2f_o$ be located in the accelerating region, the length of coupled-Schiffman section must be shorter than $L/2$. The even-mode phase velocity accelerating effect at $2 f_o$ of a shortened coupled-Schiffman section is shown as the solid-circle line in Figure 4.3. The target of $\theta_e = \theta_o = 180^o$ at $2 f_o$ can be achieved after adding a interconnecting coupled line, three coupled line corners, and a tail coupled line.
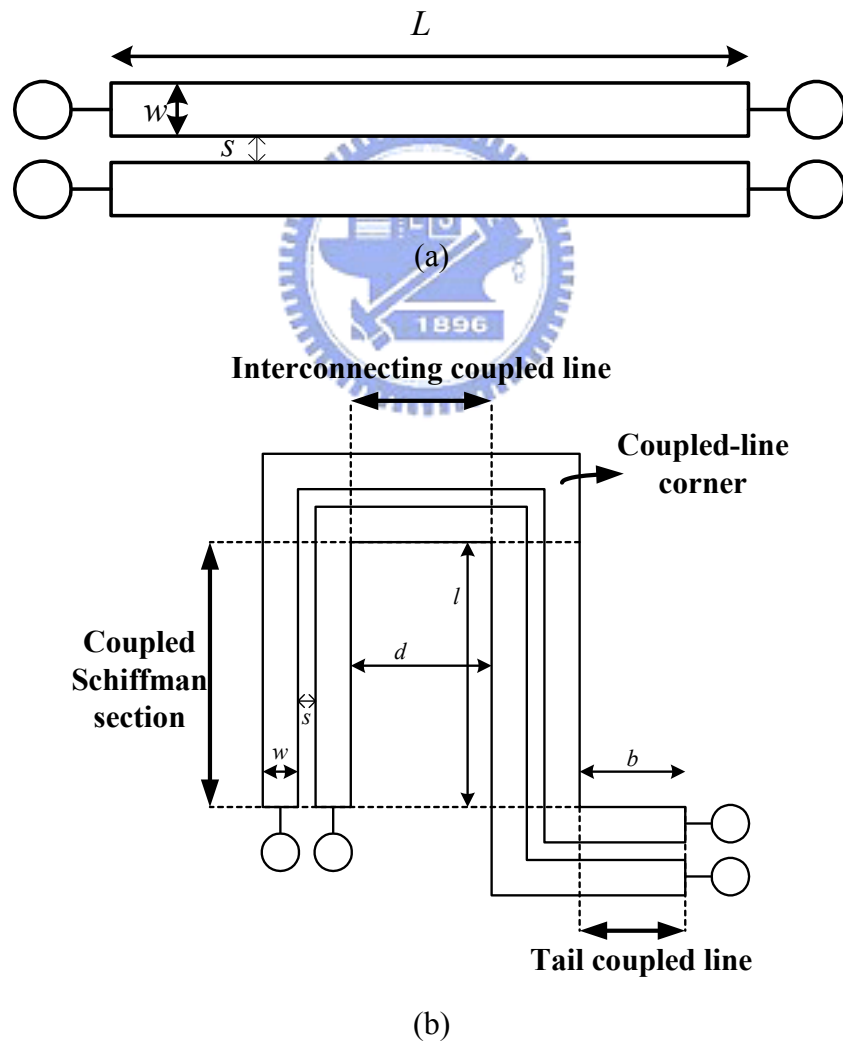
Figure 4.2   (a) The conventional parallel-coupled line. (b) The proposed meandered parallel coupled line.

47
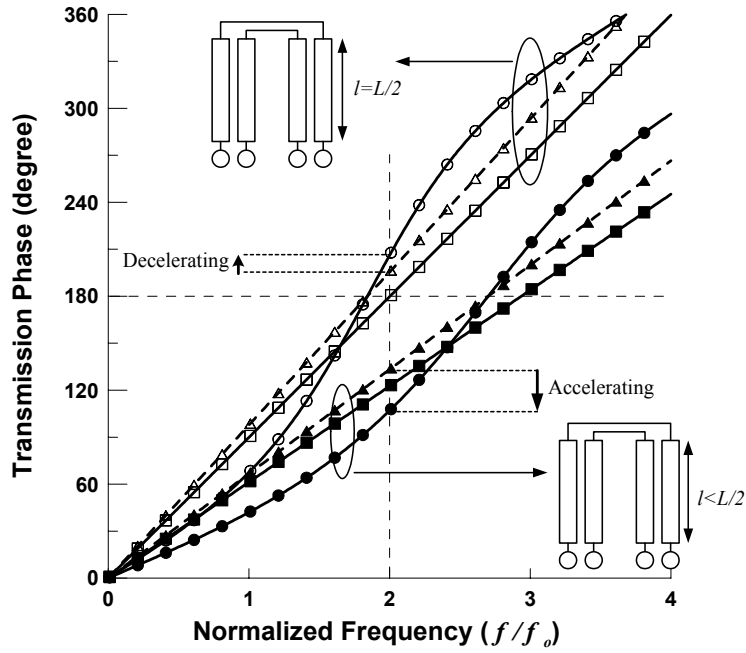
Figure 4.3   The modal transmission phases of a conventional parallel-coupled line
and a coupled Schiffman section with different coupled line length.

For $l = L/2$, —□— : θ_o, -△- : θ_e without Schiffman effect, —○— : θ_e with Schiffman effect.

For $l < L/2$, —■— : θ_o, -▲- : θ_e without Schiffman effect, —●— : θ_e with Schiffman effect.
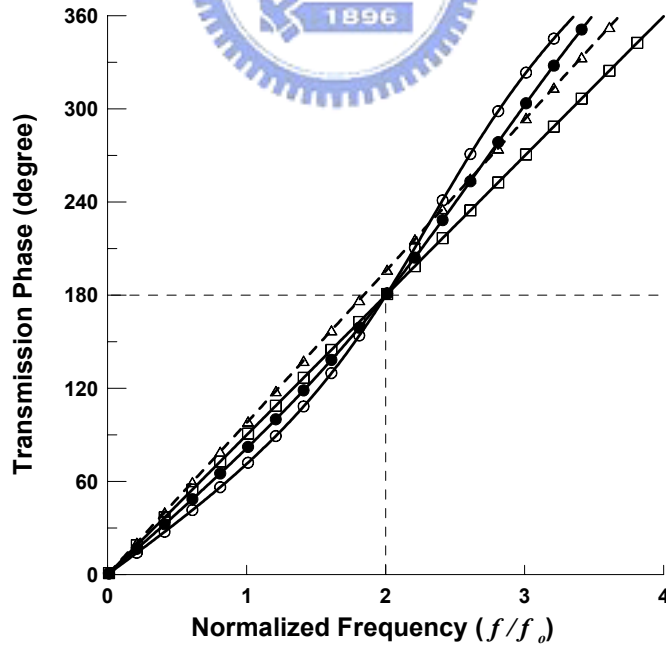
Figure 4.4   The even-mode -△- and odd-mode —□— transmission phases of a
conventional parallel-coupled line, and two different solutions —○— , and —●— of
meandered parallel coupled lines with equal modal transmission phases at $2f_o$.

48

With same w and s, there are multiple solutions of coupled-Schiffman section length l, interconnecting coupled line length d, and tail coupled line length b for $\theta_e = \theta_o = 180^o$ at $2f_o$. The hollow-circle curve and solid-circle curve in Figure 4.4 are the even-mode transmission phases of two different meandered parallel coupled lines where $\theta_e = \theta_o = 180^o$ at $2f_o$ is achieved. The reason can be briefly explained that as b is shortened, the coupled-Shiffman section length l increases and the accelerating magnitude at $2f_o$ decreases. Therefore, the meandered distance d must be shortened to compensate the reduction of accelerating magnitude. Since b and d are tunable, the layout of a proposed meandered parallel-coupled line filter can be flexibly changed to obtain a desired filter's width-to-length ratio.

4.3 Filter design

Design procedures of the proposed filter will now be discussed in this section. Here, as an example take filters passband frequency to be 1 GHz. Therefore, spurious passband at 2 GHz needs to be suppressed. The substrate is chosen with $\varepsilon_r = 10.2$ and thickness $h = 50$ mil (1.27 mm). The main reason for choosing this relatively high ε_r substrate is to challenge the relatively large deviation between V_p^e and V_p^o. This in general increases the difficulties in suppression of the spurious passband at $2f_o$.

As shown in Figure 4.2(b), the proposed meandered parallel coupled line comprises an interconnecting coupled line, a tail coupled line, a coupled-Schiffman section, and three coupled-line corners. A circuit simulator such as Agilent ADS or AWR Microwave Office can be used to analyze the behaviors of the meandered parallel coupled line. The models used in the circuit simulation are described as following. The interconnecting and tail coupled line use the standard microstrip coupled-line model in the circuit simulator. The coupled-line corners and the coupled-Schiffman section are modeled in most of circuit simulators based on look up table of EM results. Using a circuit simulator can quickly get desired design parameters with iterations. The iteration procedures are similar to those described in section 3.2. Because the constrains are different and there is an extra tail coupled line in this structure, we have to describe the constrains and the iteration procedures in detail here. Since the dimensions w, s, and d have larger weightings than l and b for the modal characteristic impedances of the meandered parallel-coupled line, we optimize w, s, and d in circuit simulator to obtain the desired modal characteristic impedances, which are corresponding to the desired bandpass response. In the optimization for modal phases, in order to make the center frequency to locate at desired frequency, the average of θ_e and θ_o should be 90° at desired center frequency.

In addition, $\theta_e = \theta_o = 180^o$ at $2f_o$ is the other constrain for suppressing the spurious passband. The dimensions d, l and b have larger weightings than w and s for the modal transmission phases of meandered parallel coupled line. The desired modal transmission phases can be obtained by optimizing d, l, and b. After several iterations, which just like the results in section 3.3 and 3.4, the exact physical dimensions of meandered parallel-coupled line with desired electrical parameters can be obtained.

As discussed in section 4.2 that tail coupled line length b can be changed. Therefore, properly choosing of b can obtain a good width-to-length ratio of the filter. For a certain b value, two design plots as those of Figure 4.5(a) and (b) can be obtained to quickly synthesize the desired filter. Because the dimensional variables and electrical variables of a meandered parallel-coupled line are too many, a set of two plots to represent them is required. Here, based on the fabricated material and constrains described in last paragraph, we arrange Figure 4.5, which are the design plots of the meandered parallel-coupled line with a chosen b. To generate the design plots as Figure 4.5(a), the tail coupled line length b can be firstly chosen. As long as b is fixed, the meandered distance d and coupled Schiffman section length l can be obtained corresponding to various w and s where the constrains of $\theta = 90^o$ at f_o and $\theta_e = \theta_o = 180^o$ at $2f_o$ are matched. It should be pointed out that because the accelerating magnitude around f_o is larger than $2f_o$ as shown in Figure 4.4, the frequency spacing between $\theta = 90^o$ and $\theta = 180^o$ is smaller than one f_o. It implies that if the filter's passband frequency is at f_o, the frequency for $\theta = 180^o$ where the spurious passband located will be a little bit lower than $2f_o$. Now, all of the physical dimensions in Figure 4.2(b) are fixed. We should know that, for same w and s, the even- and odd-mode characteristic impedances of the meandered parallel coupled-line are different from that of the conventional coupled line. Figure 4.5(b) shows the Z_{0e} and Z_{0o} versus w and s of a meandered parallel-coupled line. The particular design curves in Figure 4.5 are based on b equals to one-eightieth wavelength ($\lambda/80$, i.e. about 60mil (1.524 mm)).

After completing the design plots for a chosen b, we can use the design plots to design the proposed filter. First, for a given filter's passband parameters, sets of even- and odd-mode characteristic impedances of each coupled-line section are obtained based on TEM assumption. After that, using Figure 4.5(b), with Z_{0e} and Z_{0o} obtained in step 1, we then have the corresponding w and s. Finally, as long as the w and s are known, the corresponding d and l can be obtained in Figure 4.5(a). By cascading each meandered parallel-coupled line section, a proposed filter is finished. According to previous discussion, the filter is designed with passband at f_o and free of spurious passband at $2f_o$. The above-described design procedures based on circuit simulator

such as Agilent ADS or AWR Microwave Office can rapidly get the physical layout of the proposed filter. Final fine-tuning based on an EM simulator such as Sonnet is required to precisely eliminate the first spurious passband and to maintain the main passband performance. These design procedures can largely save the designing time compared to the method of purely using the EM simulator.
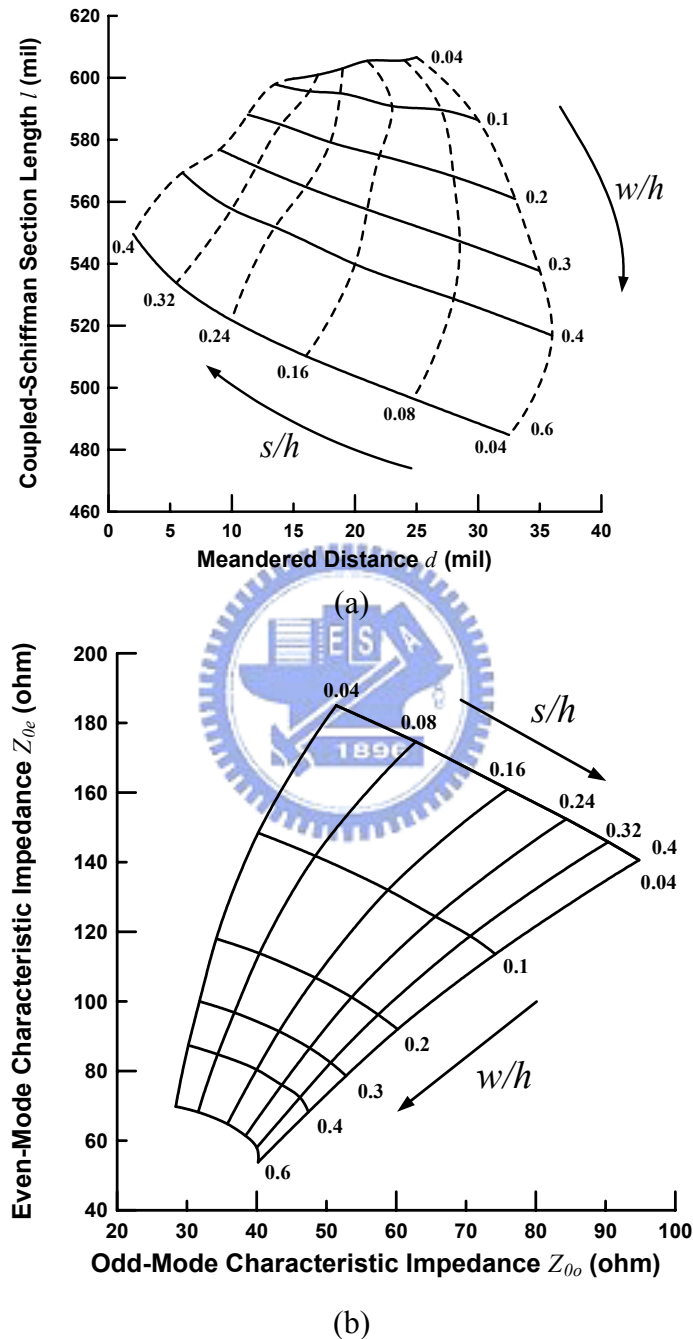

(a)

(b)

Figure 4.5   The design plots of the meandered parallel coupled line with $b = 60$ mil. (a) The corresponding meandered distance d and coupled-Schiffman section length l. (b) The even- and odd-mode characteristic impedances versus w/h and s/h of meandered parallel-coupled line.

4.4 Simulation and measurement responses

Three bandpass filters with Chebyshev response of 0.1-dB passband ripple are fabricated to demonstrate the proposed first spurious passband-free performance. The designed center frequency is 1 GHz. The circuits are fabricated on a Rogers RT/6010 substrate. The substrate has a relative dielectric constant of 10.2, a thickness of 50 mil, and a copper cladding of 0.5 oz.

Although the design procedures have been described in section 4.3, we still need to provide the following further explanation. Since the fractional bandwidth (FBW) of the filters is too large, design equations in [24] are not adequate. More accurate design procedures based on ideal TEM coupled line can be used [25]. Following these design steps, a series of Z_{0e} and Z_{0o} are obtained. We can then determine if b has a preferable filter's width-to-length ratio. After b is chosen, we can draw the design plots just like Figure 4.5(a) and (b). Using the obtained Z_{0e} and Z_{0o} values, the corresponding w and s can then be obtained in Figure 4.5(b). By using the known w and s with the design plot [see Figure 4.5(a)], the corresponding d and l, is therefore, determined. The dimensions of each meandered parallel-coupled line section can be obtained separately by the above-described procedures. We can then use the circuit simulator to do the initial verification for the obtained dimensions of the proposed filter. Finally, we use the EM simulator such as Sonnet to finalize the design.

Here, something must be remembered that when a circuit simulator is used, it is assumed that each meandered coupled-line section is independent of each other. The practical interaction, however, indeed exists. Since the equality of θ_e and θ_o is very sensitive to the external interference, slightly tuning of d and l to compensate the interaction effects is needed in the EM simulation. Empirically, 10% increasing in d and 5% increasing in l are needed. Since the even- and odd-mode characteristic impedances are insensitive to the external interference, the w and s value can be maintained.

The parameters including the specifications and detailed dimensions of each meander parallel coupled-line section of the filters are listed in Table 4.1. The simulated and measured responses are depicted in Figure 4.6, and their "b"s are all 60 mil. Two filters with order 3 and one filter with order 5 are designed. The FBW of filter A and C (order 3 and 5 respectively) is 50%, and that of B (order 3) is 30%. Since the lower edge of the first spurious passband is closer to the upper edge of main passband as the filter's FBW becomes wider, the performance of upper stopband may degrade seriously to worse than –30 dB. Therefore, wide bandwidth filter is chosen to show the impressive improvement of the upper stopband performance. Figure 4.6 (a)

shows the simulated and measured results of filter A. A conventional filter with the same specifications is also shown in Figure 4.6 (a) to compare the improvement of upper stopband performance. In Figure 4.6 (a), the upper stopband rejection is improved from –30 dB to below –50 dB and the spurious passband suppression at 2 GHz is improved form –10 dB to below –60 dB. Comparing the proposed filter to the conventional one, an excellent improvement is achieved. In Figure 4.6 (b), the filter B's upper stopband is improved to –50 dB and the spurious passband can be suppressed to approximately –55 dB. In Figure 4.6 (c), the filter C's upper stopband is improved to approximately –70 dB and the spurious passband can be suppressed to approximately –70 dB. The layouts and photographs of the filter A, B, and C are shown in Figure 4.7 and 4.8, respectively. The photograph in Figure 4.9 depicts the circuit size comparison between filter A and a conventional filter with same filter parameters. It is obvious that the circuit size is drastically reduced.

Table 4.1   Filter design parameters.

Filter	Order (n)	FBW	b (mil)	w, s, d, l of ith meandered parallel-coupled section (mil)												Overall circuit size (mil x mil)
				i=1, n+1				i=2, n				i=3, n-1				
				w	s	d	l	w	s	d	l	w	s	d	l	
A	3	50%	60	10	2	37	571	11	3	35	567					585 x 618
B	3	30%	60	7	5	27	600	7	8	22	605					523 x 649
C	5	50%	60	6.5	3	32	584	7	5	32	584	15	3	34	554	853 x 636

(a)

(b)

54
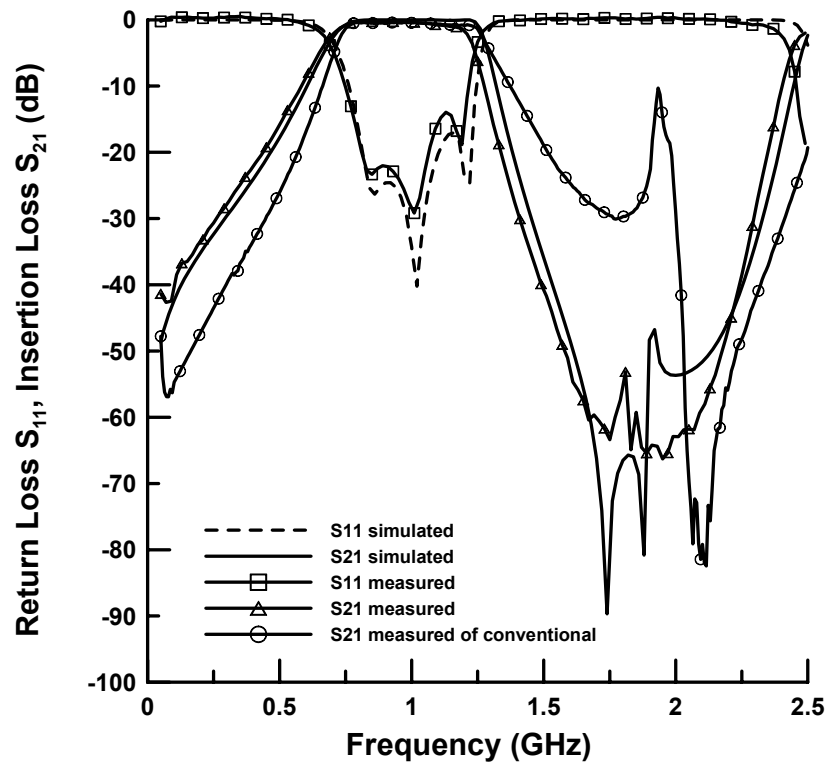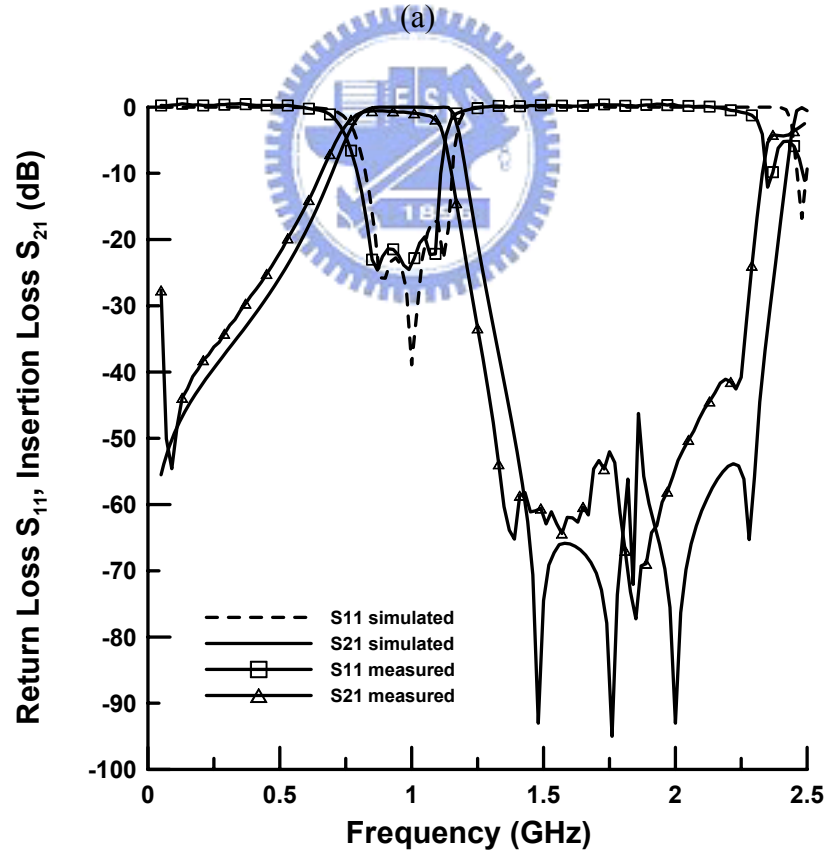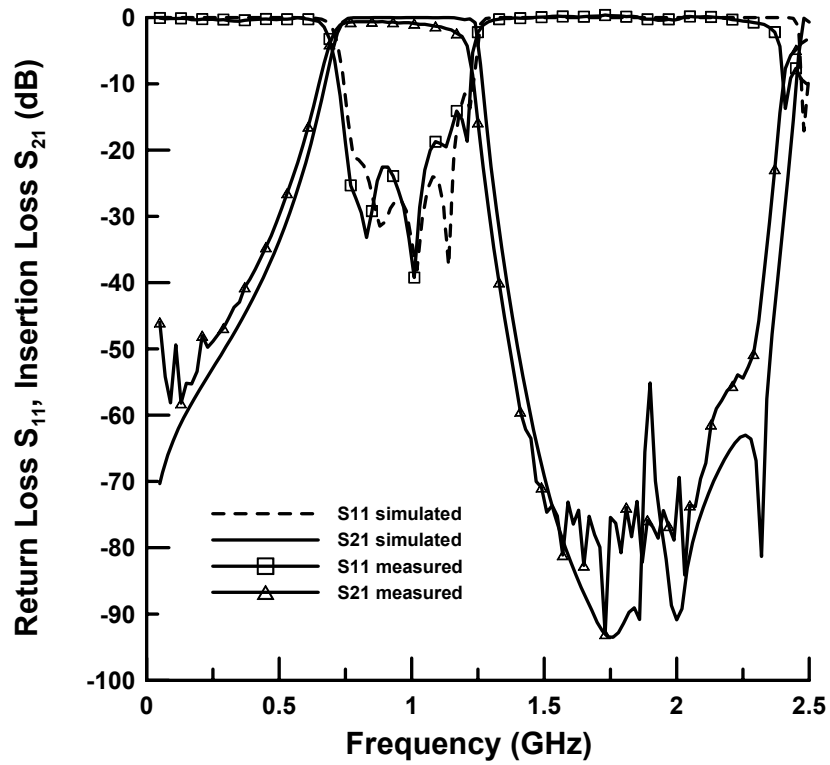
(c)

Figure 4.6 (a)The simulated and measured responses of filter A and the measured insertion loss of conventional filter with the same specification is compared. (b) The simulated and measured responses of filter B. (c) The simulated and measured responses of filter C.

(a)

(b)

(c)
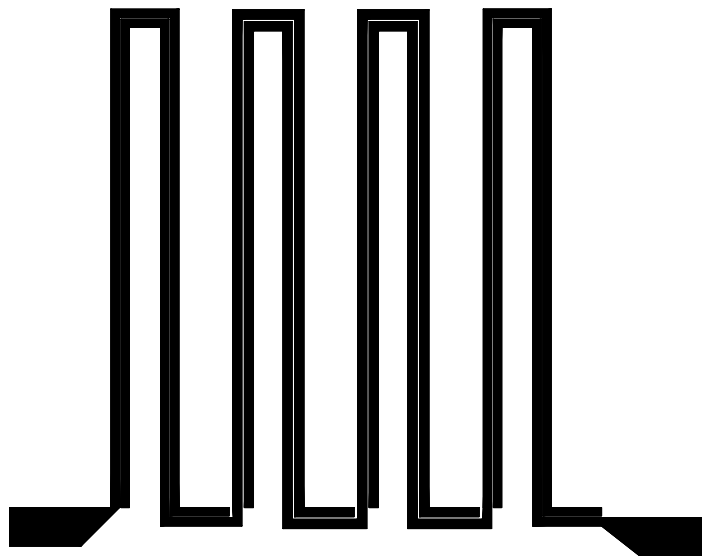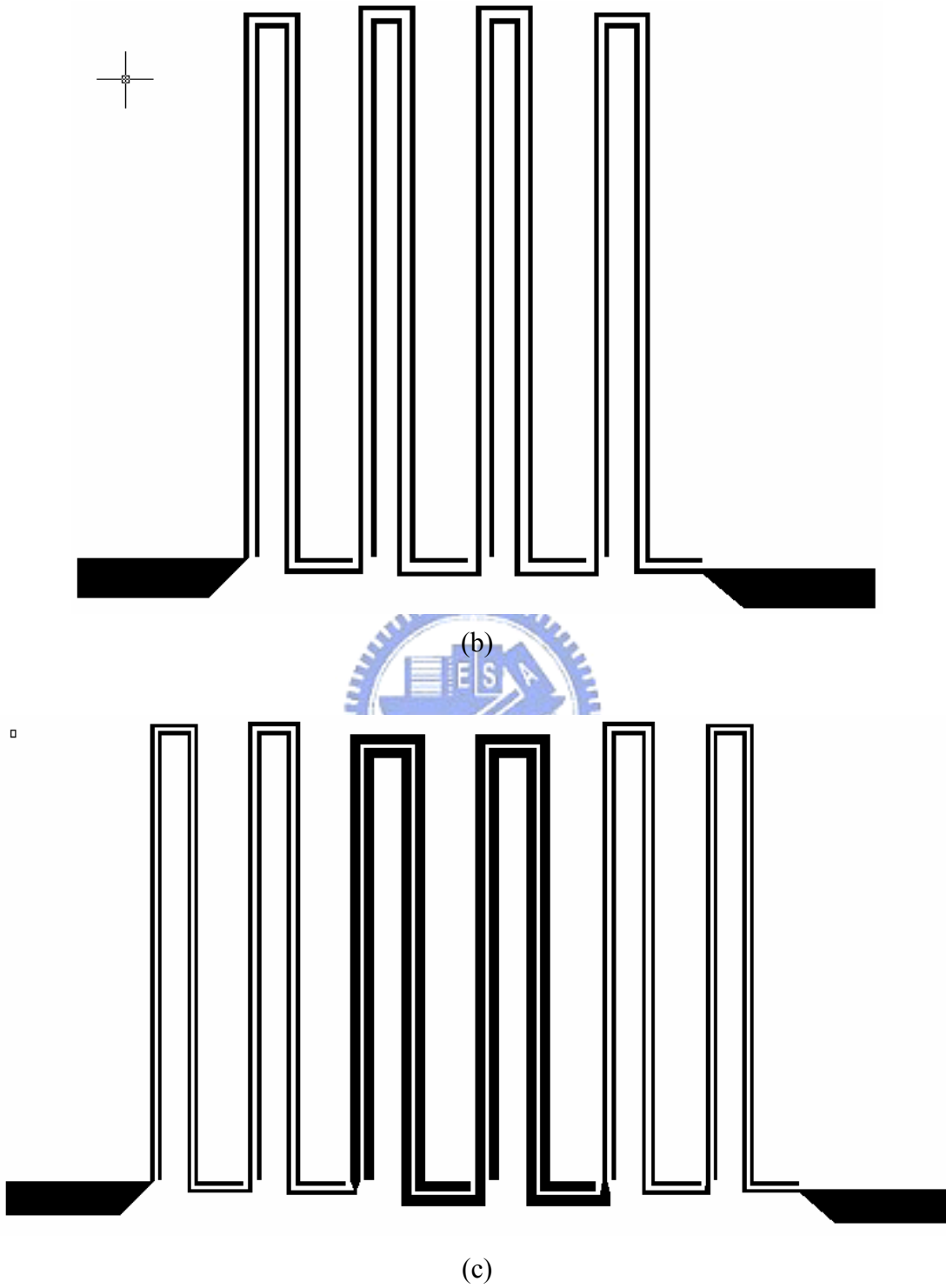
Figure 4.7   The layout of (a) Filter A. (b) Filter B. (c) Filter C.
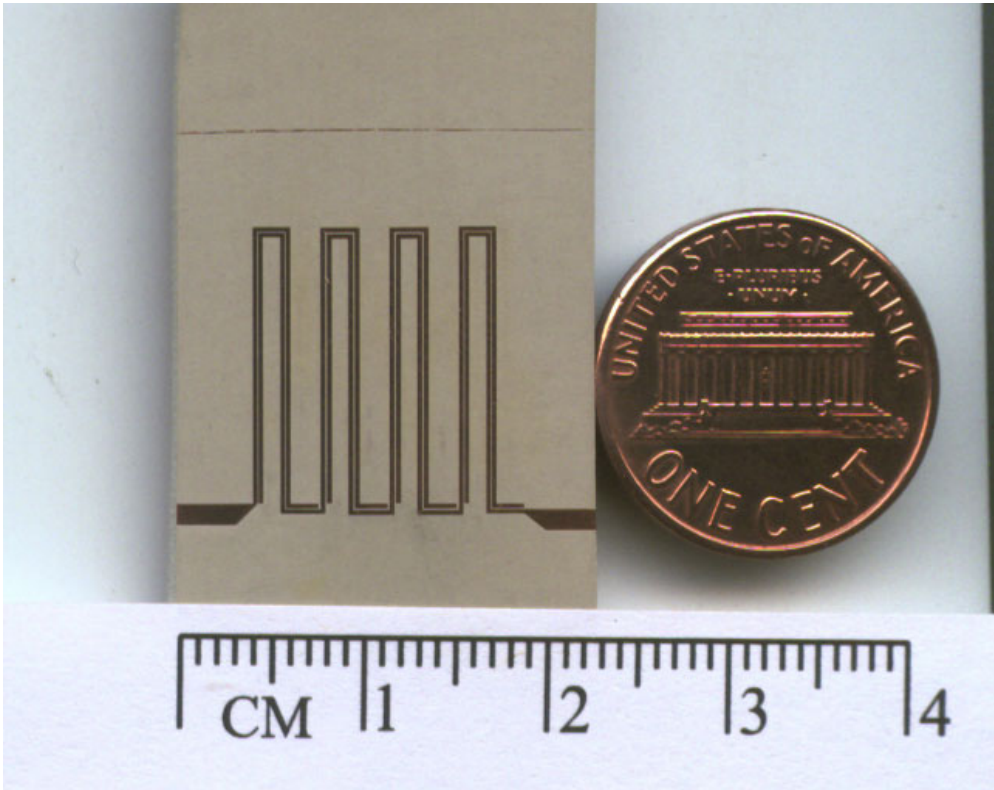
(a)
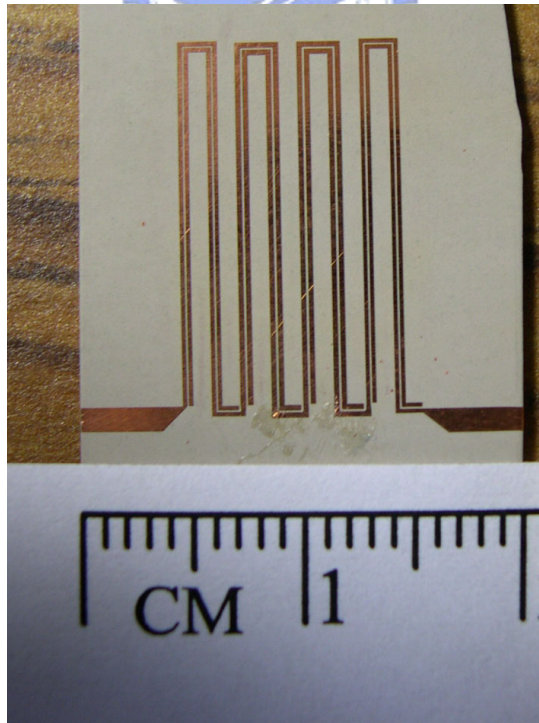
(b)
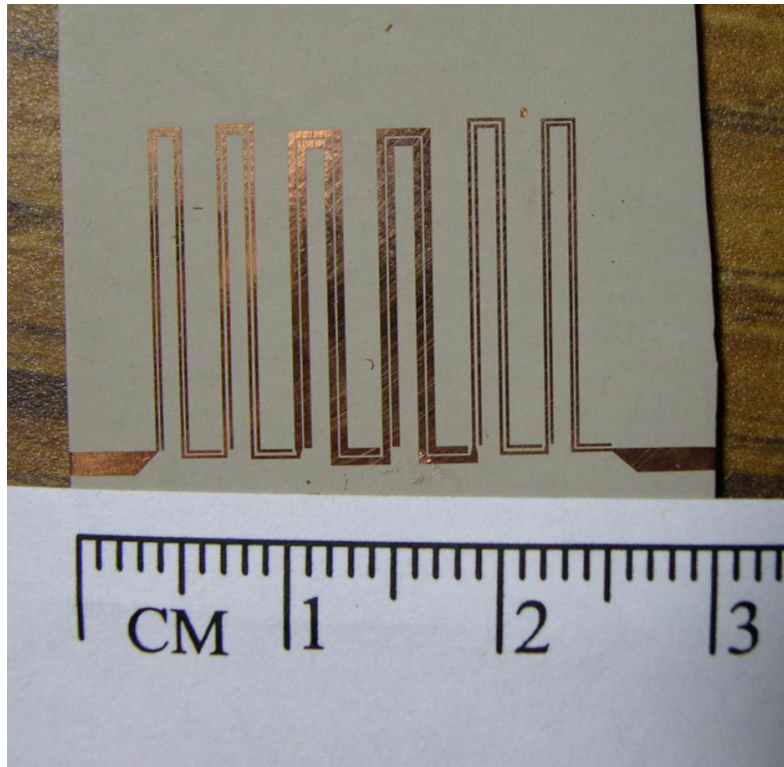
(c)

Figure 4.8   The photograph of (a) Filter A. (b) Filter B. (c) Filter C.

Figure 4.9   The circuit size comparison between filter A and conventional filter.

4.5 Discussion

If we look at the simulated insertion loss of all three filters in Figure 4.6, some transmission zeros appear in the upper stopband.   These transmission zeros are possibly due to the parasitic magnetic cross-coupling between nonadjacent resonators. The parasitic magnetic coupling is because that at the bottom of the filter every

meandered coupled-line section has strongest RF current, and this strongest current-carrying line segments are very close to the next meandered coupled-line sections. In the mean time, magnetic coupling cannot be blocked by other lines. These upper stopband transmission zeros cause the filters to display a steeper upper stopband skirt than that of lower stopband. In addition, we can observe the insertion loss at upper end of passband is a little bit larger than that of lower end. The reason is because the resonator's quality factor is finite in practical fabrication and the transmissions zeros in the upper stopband cause sharp roll off at high side skirt. The transmission zeros are not apparent in the measured curves due to their finite resonator Q value and sensitivity of the measurement equipment (the sensitivity of our equipment is approximately -70dB). All the measured results have a good agreement with the simulated results in both the passband and stopband. Summarizing the above three examples, we may conservatively conclude that the proposed meandered parallel coupled filter improves the upper stopband rejection and the spurious passband at $2f_o$ by at least 20 dB and 40 dB, respectively.

Chapter 5

Analysis, design and realization of miniaturized loose coupler with high directivity
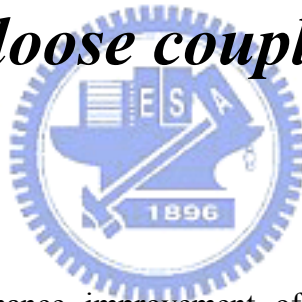
The method of performance improvement of a microstrip coupler and its applications has been discussed in previous chapters. However, the method of meandering is only applicable to relatively tight couplers. For a relatively loose coupler, there have at least two disadvantages. First, the coupled line spacing has to be large for loose coupling. This means that the circuit occupies larger space. Second, the directivity is poor or even negative value. Since the coupling gets loose and the isolation doesn't change too much with the same substrate, the directivity is very poor in a loose coupler. Many previous works focused on the directivity improvement as described in section 1.3. However, most of them are not suitable to apply to loosely coupled microstrip lines because the widely spaced lines can hardly place lumped elements and have minimal effect on the modal phase velocity by wiggling. Although some of them can shorten the coupled line length by the odd-mode slow wave effect, no studies access the reduction of coupled line spacing in loose coupler.

In this chapter, a miniaturized loose coupler with high directivity is proposed. By inserting split grounded strips in the middle of two coupled microstrip lines, we can block the coupling electromagnetic field and reduce the coupled line spacing. The

directivity is improved by placing two interdigital capacitors across the edges of two coupled lines. The topology of grounded strip and realization of interdigital capacitor are discussed. The design procedures with commercial circuit simulator and EM simulator are described in detail. And two example couplers are designed and implemented to demonstrate the feasibility of the proposed method.

5.1 The placement of grounded strip

As shown in Figure 5.1, it is well known that a grounded strip can block the coupling electromagnetic field between two coupled lines and reduce coupling. Moreover, the effect is more obvious as the area of grounded strip becomes larger. Base on this effect, the loose coupler can be achieved with a smaller coupled lines spacing. However, because the grounded strip is a two ends short-circuited resonator too, it has its self-resonance frequency. As the self-resonance frequency falls into the operation band of the coupler, the responses of the coupler would resonate at that frequency, then, the coupler's performance is destroyed. Since the grounded strip must exist, the only way to solve this problem is to raise the self-resonance frequency. Shortening the length of grounded strip can effectively raise the self-resonance frequency. However, shortening the length too much would greatly reduce the field-blocking capability. Reducing the strip width can slightly decrease the effective dielectric constant and increase the resonant frequency of the grounded strip. In order to keep the field-blocking capability, the original thicker grounded strip can be split into two strips as shown in Figure 5.2. The split grounded strips keep the field-blocking capability. Although the later is somewhat ineffective than the former in the raising of self-resonance frequency, it still provides appropriate improvement, especially in the case of loose coupler, in which a very wide grounded strip is needed.

Here, we chose ceramic substrate with relative dielectric constant of 9.8 to verify the proposed method. For the similar reason as previous chapters, a relatively high dielectric constant substrate is chosen to demonstrate the feasibility of proposed method even in the more difficult situation. The conventional via hole cannot be used to ground the two ends of the strip because via hole is not a standard process in ceramic substrate that we chosen for this design. There are two methods to ground the strips. First, virtually grounds the strip by a $\lambda/4$ open stub. Second, grounds the strip by wrap-around grounding strips or by grounded metal posts located at the side of the circuit. Figure 5.3(a) and (b) show the methods of grounding. The method in Figure 5.3(a) is often used in microwave circuit design, but introducing of $\lambda/4$ open stub increases the effective length of the grounded strip and then drastically decreases the self-resonance frequency. Therefore, this method is not appropriate. The second

method does not have this problem it is a standard process in thin film circuits with ceramic substrate inherently. Thus, the second method is adopted.
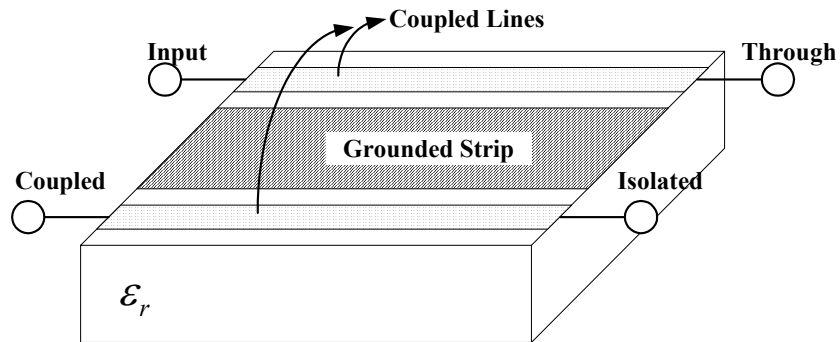

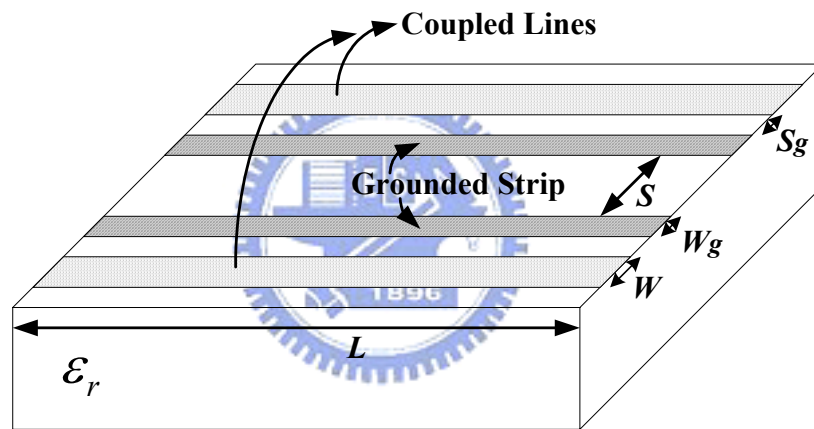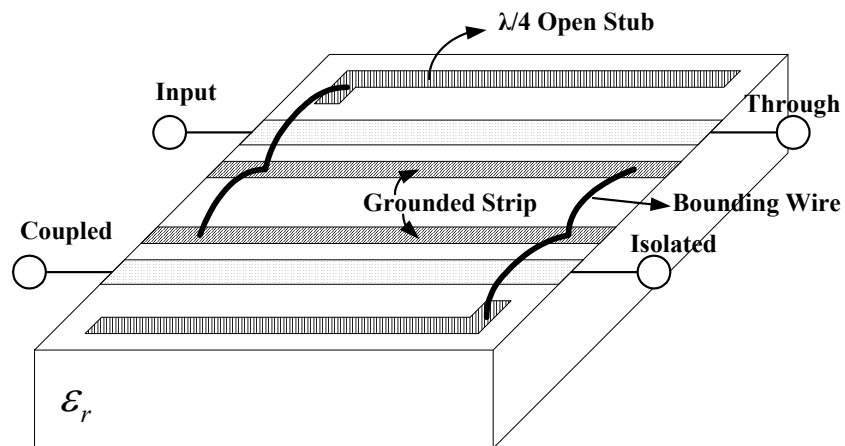Figure 5.1   Coupled lines with a grounded strip insertion.

Figure 5.2   Coupled lines with a modified grounded strip.

(a)
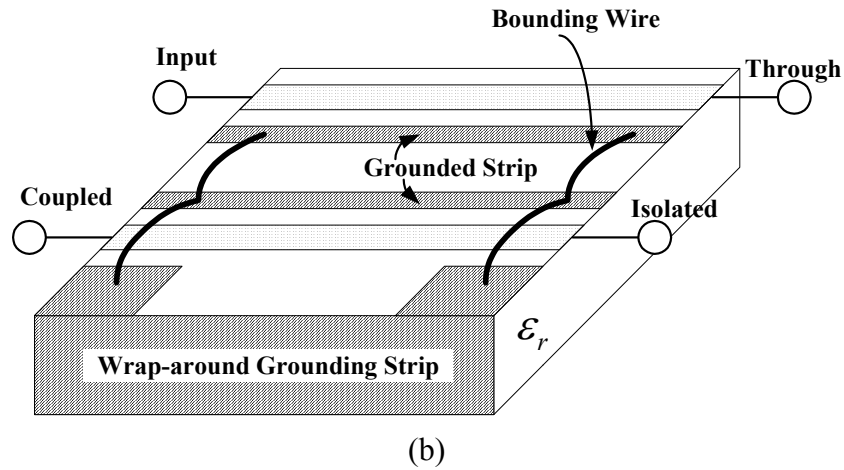
Figure 5.3   The grounding effect is induced by (a) λ/4 open stub and (b) wrap-around grounding strips.

5.2 Procedures of implementation

The coupler with split grounded strips is shown in Figure 5.2, where W is the coupled line width, S_g is the spacing between coupled line and grounded strip, W_g is the grounded strip width, S is the spacing between the two split grounded strips, and L is the coupled line length. In order to simplify the design variables, we fixed the W_g and S_g. Therefore, W and S decide the coupled line's even- and odd-mode characteristic impedance, Z_{0e} and Z_{0o}. The L is decided according to the center frequency f_o. Besides, S_g must be as small as possible in order to maximize the field-blocking capability, and W_g is a compromise between field-blocking capability and self-resonance frequency. After considering the process limitations, we fixed the S_g and W_g to be 4 and 6 mils respectively.

We use the circuit simulator such as AWR Microwave Office to extract the initial physical dimensions of the coupler. As shown in Figure 5.5, the coupler is divided into three sections. Both the left and the right section use standard microstrip coupled line model in the circuit simulator, and the middle section uses the microstrip 4-coupled line model, which is modeled in most of circuit simulator based on look up table of EM results. In order to reserve the space for the compensating capacitors, the length of both left and right sections are set to be 0.05L, and the middle section is 0.9L. As mentioned before, the S_g and W_g are 4 and 6 mils respectively. Appropriate tuning W and S can obtain the targets of desired loose coupling value and 50 Ohm ports impedance value. The center frequency f_o is controlled by L.

On the other hand, although the compensating capacitors can improve the

directivity, they also affect the coupling value (this is more evident as the coupling becomes looser) and center frequency. This phenomenon would consume more tuning time in later EM simulation. In order to avoid this problem, we must pre-consider the effect of the compensating capacitors in the initial-guess stage. Since the coupling would increase 2 to 5 dB after adding the compensating capacitors, we purposely make the coupling 3 dB less than the desired coupling value. On the other hand, because the even mode transmission phase is nearly not affected by the compensating capacitors, the even-mode transmission phase of 90° is taken as the center frequency.

According to above descriptions, we can extract the appropriate dimensions in initial stage. Then, we use EM simulator Sonnet to verify these circuit dimensions where the compensating capacitors are not involved. After the first tuning, we can get the S-parameters that are corresponding to proper circuit dimensions. Then, put the S-parameters back to the circuit simulator to estimate the even- and odd-mode transmission phase. The compensating capacitor C can then be calculated from [7]:

$$C = 1/(4\pi f_o Zoo \tan\theta_r) \tag{5.1}$$

where

$$\theta_r = \sqrt{\varepsilon^o_{r\_eff} / \varepsilon^e_{r\_eff}} \, \pi/2 \tag{5.2}$$

and $\varepsilon^o_{r\_eff}$ and $\varepsilon^e_{r\_eff}$ are, as described in section 2.1, the even- and odd-mode effective dielectric constant, respectively. Even thought the equations are not accurate enough for loosely coupled lines, they are still a good starting point for optimization. From circuit simulator, the appropriate lumped circuit capacitor value can be obtained. Here, as shown in Figure 5.4, we use interdigital capacitor to implement the compensating capacitors. We fixed the finger spacing and finger width to be 2 to 4 mils due to process limitations. Then, we use the formulas described in [38] to estimate the initial values of the finger number (finger number is defined as total strip number in the overlap region) and finger overlapping length. Finally, the interdigital capacitors are involved in the previously obtained coupler's dimensions while doing EM simulation. After fine-tuning the design of high-directivity loose coupler is finished.
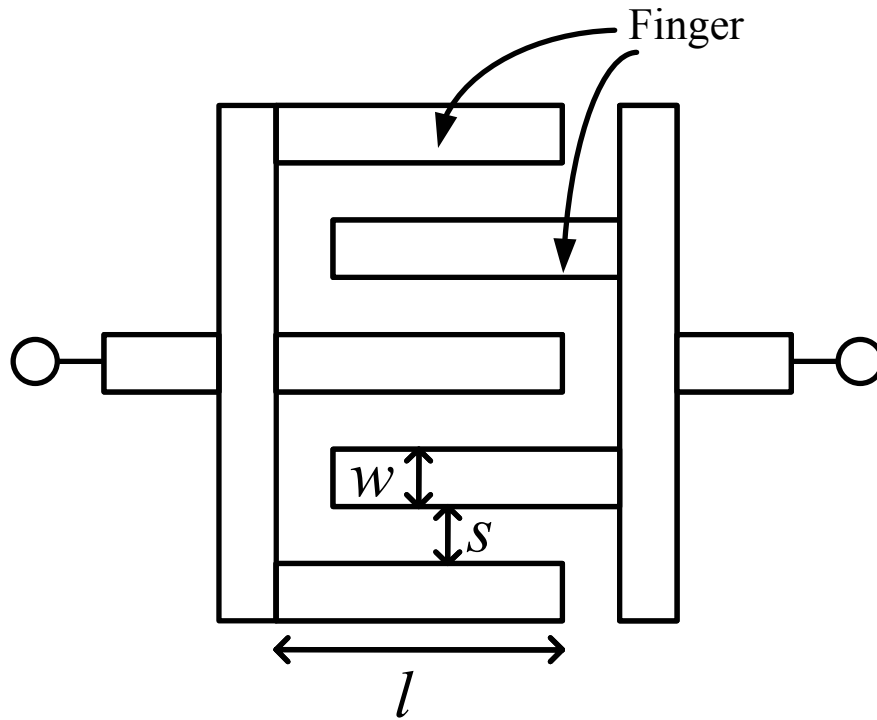
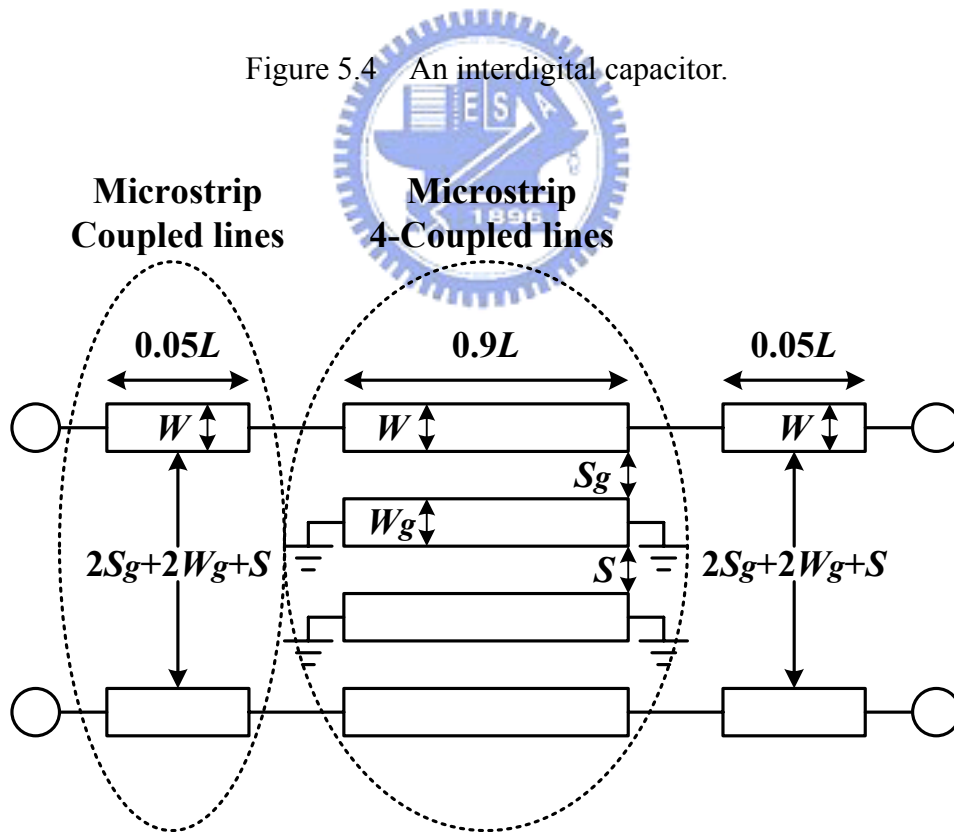Figure 5.4   An interdigital capacitor.

Figure 5.5   The extraction of initial physical dimensions of coupler in circuit simulator.

5.3 Simulation and measurement

Design procedures of the proposed coupler are discussed in the previous section. Here, take the 30- and 40-dB couplers with center frequency of 2 GHz as examples. The ceramic substrate is chosen with $\varepsilon_r = 9.8$ and thickness $h = 15$ mil (0.381mm). The reason why we choose this high ε_r substrate is similar to previous chapters that we want to challenge the difficulty of relatively large deviation between V_p^e and V_p^o. Inherently, larger phase velocity difference causes worse directivity.

The simulated and measured results of 30-dB coupler are shown in Figure 5.6 (a) and (b), respectively. The measured coupling is 28.4dB and directivity is 25.2dB. The measured responses show a 1.6-dB of coupling value raising and a more than 10-dB directivity degradation. The directivity degradation may be from process tolerance of capacitor because the finger width and spacing in the 30-dB coupler is chosen to be 2 mils. The simulated and measured results of 40-dB coupler are shown in Figure 5.7 (a) and (b), respectively. All of the simulated and measured responses are matched perfectly except a 1.5-dB of coupling value raising. The measured directivity is in good agreement with simulated one due to the finger width and spacing is chosen to be 4mil so that the relative etching tolerance reduces. It should be point out that both couplers show smaller coupled-line spacing than conventional one due to the insertion of grounded strips and depict a smaller coupled-line length because of the slow wave effect caused by compensating capacitors. Consequently, the area of both couplers is smaller than conventional loose coupler with the same coupling value. The detailed dimensions of both couplers are listed in Table 5.1. In Table 5.1, we can discovery the W_g of 40-dB coupler is tuned to 14 mils. In this case, because 6-mils W_g is not available to block the coupling to be 40 dB, in order to not increase coupled-line spacing S too much and keep the resonance frequency is still high enough, we slightly increase W_g to make the coupling can be as loose as 40 dB. The photographs of the 30- and 40-dB coupler are shown in Figure 5.8 (a) and (b), respectively.

Table 5.1   The desired parameters of proposed couplers.

Coupling value	Designed dimensions of proposed coupler (mil)					Designed parameters of interdigital coupler (mil)				Comparison of total coupled line spacing	
							Finger's			Proposed coupler	Conventional coupler
	W	Sg	Wg	S	L	Number	Width	Spacing	Overlapping length		
30 dB	10	4	6	18	368	2	2	2	27	38	48
40 dB	10	4	14	30	370	2	4	4	6	66	145

(a)
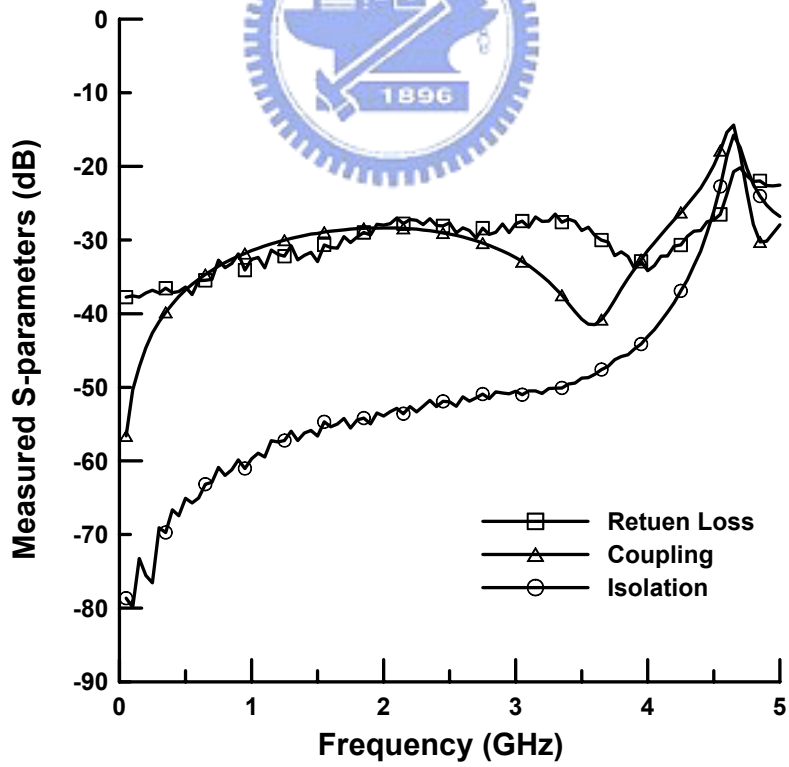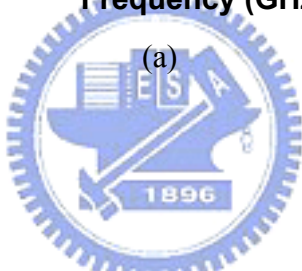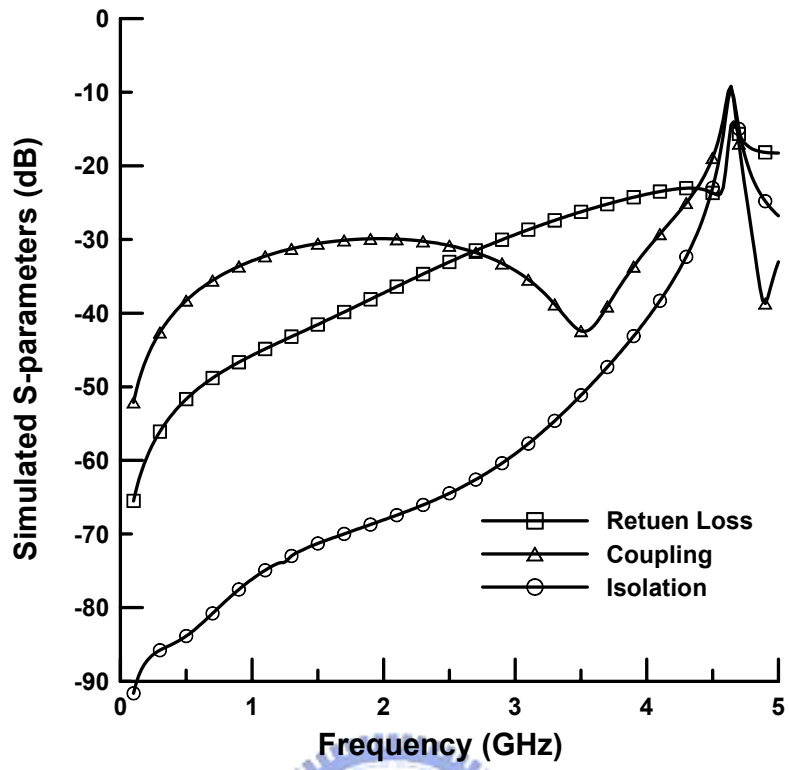
(b)

Figure 5.6   The (a) simulated and (b) measured responses of 30-dB coupler.
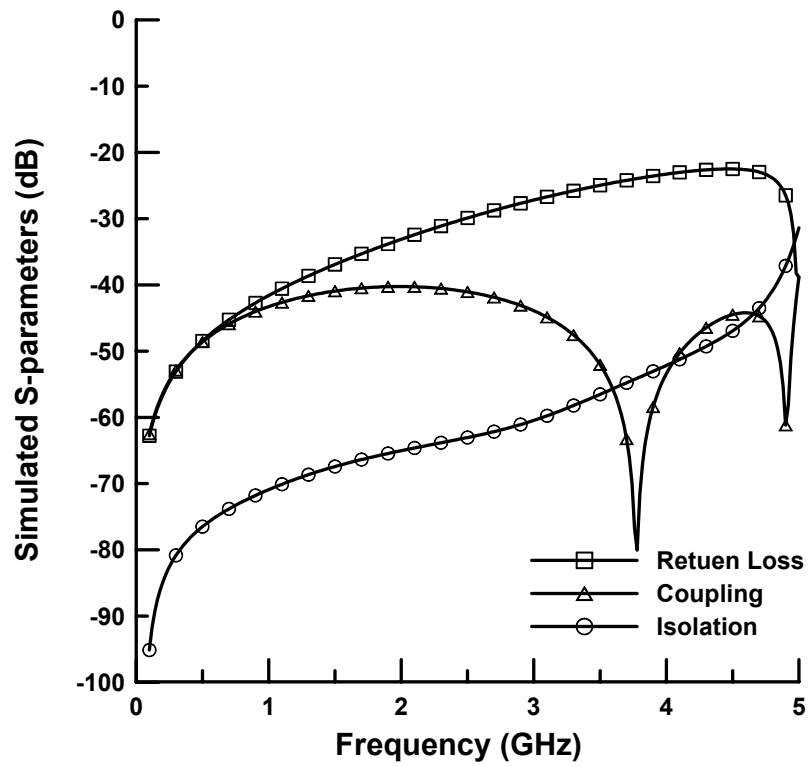
(a)
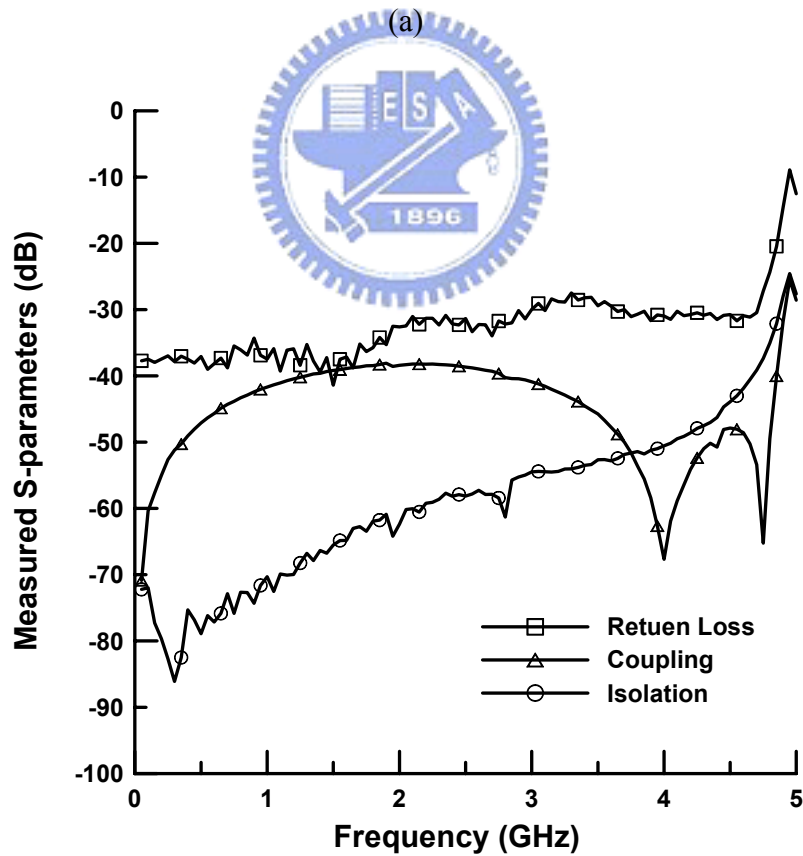
(b)

Figure 5.7   The (a) simulated and (b) measured responses of 40-dB coupler.
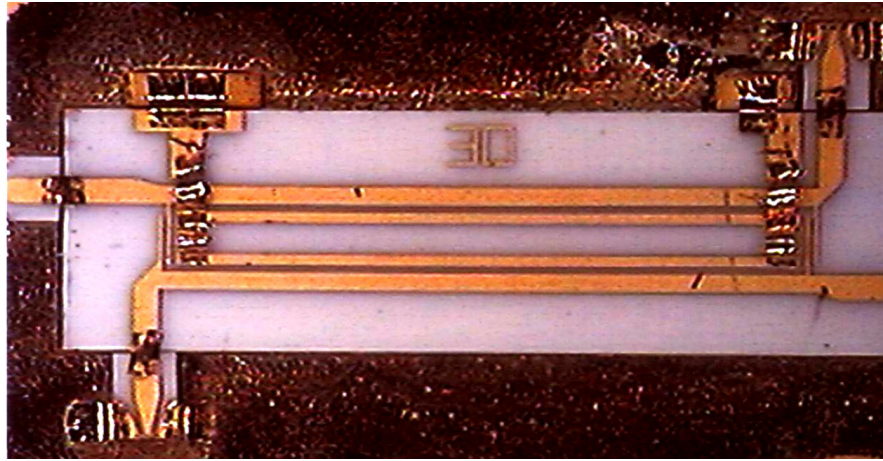
(a)
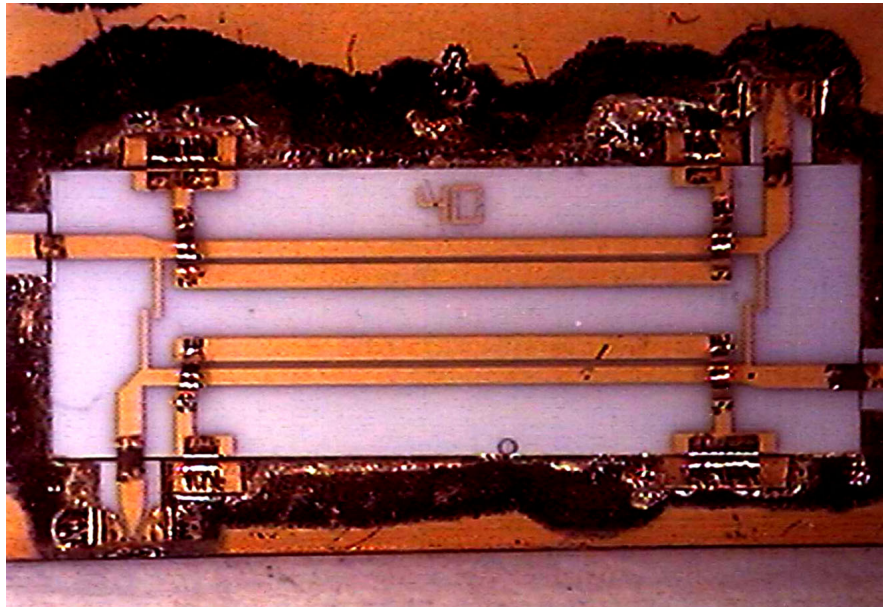
(b)

Figure 5.8   The photographs of (a) 30-dB and (b) 40-dB coupler.

5.4 Discussion

There are tiny coupling values raising (1.5 and 1.6dB) in the measured results. We firstly guess that the error might be from two possible simulation errors, finite PEC Box and zero metal thickness. The PEC box in EM simulation has finite dimensions but practically the circuit is in open space. Thus, we extend the PEC Box to be 11 times of coupler length and width for eliminating the Box effect, but the coupling is still unchanged. On the other hand, since the metal thickness is set zero in
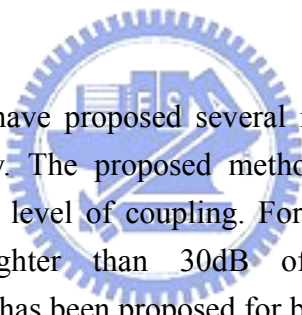
our original EM simulation, we modify it to the value of practical metal thickness, 0.15 mils. However, the coupling is still not corrected. Thus, we conservatively guess the raise of measured coupling value comes from fabrication (physical dimensions) and physical parameter (dielectric constant, substrate thickness, etc.) tolerances. In addition, in the case of 30-dB coupler, the width and spacing of the finger are chosen to be 2 mils that are the most precise scale in the whole coupler. From the measured results, 10-dB directivity degradation is observed, which implies the fabricated interdigital capacitance is not accurate enough due to the process tolerance. Therefore, the process is also an important consideration in circuit design step.

Finally, we can clearly observe that the resonant peak located near 5 GHz for both couplers. As described previously this resonance is caused by split grounded strips. Therefore, appropriate control of the width and length of split grounded strips to exclude the resonance from our desired frequency band is very important.

Chapter 6

Conclusions

In this dissertation, we have proposed several methods to obtain a microstrip coupler with good directivity. The proposed method can improve the microstrip coupler's directivity with any level of coupling. For a coupler with relatively tight coupling (approximately tighter than 30dB of coupling), the meandered parallel-coupled line structure has been proposed for both narrow band and broadband application. For a coupler with relatively loose coupling (approximately looser than 30dB of coupling), the miniaturized loose coupler structure has been proposed. Besides, we have successfully applied this high directivity coupler to a parallel-coupled filter. The proposed filter can not only shrink the size but also eliminate the first spurious passband near twice of the main passband center frequency. The methods proposed in this dissertation are summarized as follows.

6.1 Meandered parallel-coupled line

We fold a microstrip parallel-coupled structure to improve the inherent poor directivity and shorten the circuit size simultaneously. The even-mode phase velocity can be speeded up to match that of the odd-mode at any desired frequency by properly folding the parallel-coupled line. The characteristics of the proposed structure have been explained clearly and the synthesis procedures have also been described in detail. Base on the proposed structure and design procedures, a single meandered section

coupler has been successfully developed to improve the directivity drastically within a narrow band. In this case, the even-mode phase velocity is speeded up and matches to the odd-mode phase velocity at center frequency and generates an isolation zero. Therefore, the isolation deep is very high. An excellent improvement of directivity is observed in EM simulation, and at least 40dB improvement of directivity has been obtained in experiments.

In addition, in order to achieve nearly ideal TEM directional coupler performance over a bandwidth of 0 to $2f_o$, we modify the single meandered-section coupler to be a multisection one. The idea of speeding up the even-mode phase velocity by coupled-Schiffman section and straightening the dispersion of even-mode phase angle by dividing the coupler to multiple meandered parallel-coupled-line sections was proven to be successful. The even- and the odd-mode phase velocity are almost equal in a wide bandwidth of 0 to $2f_o$, thus high isolation in a wide bandwidth is got. The design procedures have been described in detail. Good agreement of simulated and measured results has been achieved. Finally, the proposed coupler has shown an excellent isolation of 50 dB over a bandwidth of 0 to $2f_o$.

Finally, we use the speeding effect of coupled-Schiffman section to equal the modal phase velocities at $2f_o$. Then the spurious passband at $2f_o$ can be suppressed. Three filters based on the meandered parallel-coupled line structure have successfully suppressed the spurious passband at $2f_o$ and reduced their circuit size. By properly adjust the physical dimensions of the meandered parallel-coupled line section, an equal even- and odd-mode transmission phases at $2f_o$ can be achieved. For a desired length to width ratio of the filter, a proper tail coupled line length can be firstly chosen. Furthermore, the structure can be analyzed quickly with good accuracy by a commercial circuit simulator. The design plots corresponding to a chosen tail coupled line length are provided for easy design. The filter design procedures based on this proposed structure have been described in detail. Good agreement of simulated and measured results has been achieved. Finally, the proposed filters have shown more than 50 dB spurious passband suppression at $2f_o$ and a much higher upper stopband rejection than those of the conventional filters has achieved.

All the experimental results verify the validity of the proposed meandered parallel-coupled line structure.

6.2 Miniaturized loose coupler

As the coupling becomes looser than approximately 30dB the layout of meandered parallel-coupled line structure becomes impossible. To solve this problem, we have proposed split grounded strips to place in the middle of two coupled

microstrip lines so that the coupling electromagnetic field is blocked and the coupled-line spacing is reduced. To place the proposed split ground strips make it possible to add modal velocity-compensation interdigital capacitors to improve the directivity. The design procedures of the proposed coupler have been described in detail. Two couplers with 30- and 40-dB loose coupling have been designed at center frequency of 2 GHz as examples. The measured performances have shown good agreement with the simulated one. Therefore, the proposed method has been proven to be a feasible way to implement a high directivity loose coupler with compact size.

6.3 Review and the future works

From the view point of physical dimensions, the proposed meandered parallel coupled line owns an asymmetric outline. That makes the circuit will be always with two kinds of propagation modes whether even- or odd-mode signal is excited. Although the mode conversion exists, it is not strong enough to disturb our analysis based on even- and odd-modes. It, however, can be treated more rigorously in the future. Therefore the analysis model should be modified and a modified equivalent circuit for the proposed structure is needed. That will make the analysis result more accurate.

In the future work, the proposed meandered parallel coupled structure can be applied to the miniaturized microstrip coupler which is inserted a grounded strip. Base on this idea, a loose coupler can not only reduce the coupled-line spacing by grounded strip but also shorten the coupled-line length and get high directivity by meandering. It is a new topic what we will go. In addition, the coupler with TEM-like behavior can be extended to a Machand type balun with broadband and good balance. In band pass filter applications, a filter can be design to free off $2f_o$ and $4f_o$ based on the proposed mechanism. About the $3f_o$, other method should be induced to suppress or remove it. These are some future works of this research.

References

[1] H. A. Affel, "High frequency signal system," U.S. Patent 1,615,896, Feb. 1, 1927.

[2] H. A. Wheeler, "Directional coupler," U.S. Patent 2,606,974, Aug. 12, 1952.

[3] S. B. Cohn, R. Levy "History of microwave passive components with particular attention to directional couplers," *IEEE Trans. Microwave Theory Tech.*, vol. 32, no. 9, pp. 1046-1054, Sep. 1984.

[4] G. L. Matthaei, L. Young, and E. M. T. Jones, *Microwave Filters, Impedance-Matching networks and Coupling Structures*, Norwood, MA: Artech House, 1980

[5] G. Schaller, "Optimization of microstrip directional couplers with lumped capacitors," *Arch. Elek. Uebertrag. Tech.*, vol. 31, pp. 301-307, July-Aug. 1977.

[6] C. Kajfez, "Raise coupler directivity with lumped compensation," *Microwaves*, vol. 27, pp. 64-70, Mar. 1978.

[7] S. L. March, "Phase velocity compensation in parallel-coupled microstrip," in *IEEE MTT-S Symp. Dig.*, 1982, pp. 410-412.

[8] M. Dydyk, "Microstrip directional couplers with ideal performance via single-element compensation," *IEEE Trans. Microwave Theory Tech.*, vol. 47, no. 6, pp. 956-964, June 1999.

[9] S. Al-taei, P. Lane and G. Passiopoulos, "Design of high directivity directional couplers in multilayer ceramic technologies," in *IEEE MTT-S Symp. Dig.*, 2001, pp. 51-54.

[10] Y. S. Lee, "Mode compensation applied to parallel-coupled microstrip directional filter design," *IEEE Trans. Microwave Theory Tech.*, vol. 22, no. 1, pp. 66-69, Jan. 1974.

[11] B. Sheleg and B. E. Spielman, "Broad-band directional couplers using microstrip with dielectric overlays," *IEEE Trans. Microwave Theory Tech.*, vol. 22, no. 12, pp. 1216-1220, Dec. 1974.

[12] C. Buntschun, "High directivity microstrip couplers using dielectric overlays," in *IEEE MTT-S Symp. Dig.*, 1975, pp. 125-128.

[13] D. D. Paolino, "MIC overlay coupler design using spectral domain techniques," *IEEE Trans. Microwave Theory Tech.*, vol. 26, no. 9, pp. 646-649, Sep. 1978.

[14] L. L. Klein, and K. Chang, "Optimum dielectric overlay thickness for equal even- and odd-mode phase velocities in coupled microstrip circuits," *Electronics Letters*, vol. 26, no. 5, pp. 274-276, Mar. 1990.

[15] K. Li, "Dielectric loaded microstrip couplers for microwave integrated circuits," in *Proc. IEEE Asia-Pacific Microwave Conf.*, 1990, pp. 1041-1044.

[16] A. Podell, "A high directivity microstrip coupler techniqe," in *IEEE MTT-S Symp. Dig.*, 1970, pp. 33-36.

[17] F. C. de Ronde, "Recent developments in broadband directional couplers on microstrip," in *IEEE MTT-S Symp. Dig.*, 1972, pp. 215-217.

[18] F. C. de Ronde, "Wide-band high directivity in mic proximity couplers by planar means," in *IEEE MTT-S Symp. Dig.*, 1980, pp. 480-482.

[19] S. Uysal and H. Aghvami, "Synthesis, design, and constriction of ultra-wide-band nonuniform quadrature directional couplers in inhomogeneous media," *IEEE Trans. Microwave Theory Tech.*, vol. 37, no. 6, pp. 969-976, Jun. 1989.

[20] D. K. Y. Lau, S. P. March, L. E. Davis, and R. Sloan, "Simplified design technique for high-performance microstrip multisection couplers," *IEEE Trans. Microwave Theory Tech.*, vol. 46, no. 12, pp. 2507-2513, Dec. 1998.

[21] J. Lin, "A study of microstrip coupler with high directivity," in *ICMMT Proceeding*, Aug. 1998, pp. 905-908.

[22] M. Kirschning and R. H. Jansen, "Accurate Wide-Range Design Equations for the Frequency-Dependent Characteristic of Parallel Coupled Microstrip Lines," *IEEE Trans. Microwave Theory Tech.*, vol. 32, no. 1, pp. 83-90, Jan. 1984.

[23] B. M. Schiffman, "A new class of broadband microwave 90° phase shifter," *IRE Trans. Microwave Theory and Tech.*, vol. 6, pp. 232-237, Apr. 1958

[24] D. M. Pozar, *Microwave Engineering,* 2nd ed. New York: Wiley, 1998, pp. 478.

[25] S. B. Cohn, "Parallel-coupled transmission-line-resonator filters," *IRE Trans. Microwave Theory Tech.*, vol. 6, pp. 223-231, Apr. 1958.

[26] G. L. Matthaei, "Design of wide-band (and narrow-band) band-pass microwave filters on the insertion loss basis," *IRE Trans. Microwave Theory Tech.*, vol. 8, pp. 580-593, Nov. 1960.

[27] C.-Y. Chang and T. Itoh, "A modified parallel-coupled filter structure that improves the upper stopband rejection and response symmetry," *IEEE Trans. Microwave Theory Tech.*, vol. 39, pp. 310-314, Feb. 1991.

[28] A. Riddle, "High performance parallel coupled microstrip filters," in *IEEE MTT-S Symp. Dig.*, 1988, pp. 427-430.

[29] D. M. Pozar, *Microwave Engineering*, 2nd ed. New York: Wiley, 1998, pp. 474-485.

[30] J.-T. Kuo, S.-P. Chen, and M. Jiang, "Parallel-coupled microstrip filters with over-coupled end stages for suppression of spurious responses," *IEEE Microwave Wireless Comp. Lett.*, vol. 13, pp. 440-442, Oct. 2003.

[31] B. Easter and K. A. Merza, "Parallel-coupled-line filters of invented-microstrip and suspended-substrate MIC's," in *11th Eur. Microwave Conf. Dig.*, 1981, pp.

164-167.

[32] I. J. Bahl, "Capacitively compensated high performance parallel coupled microstrip filters," in *IEEE MTT-S Symp. Dig.*, 1989, pp. 679-682.

[33] J.-T. Kuo, M. Jiang, and H.-J. Chang, "Design of parallel-coupled microstrip filters with suppression of spurious resonances using substrate suspension," *IEEE Trans. Microwave Theory Tech.*, vol. 52, pp. 83-89, Jan. 2004.

[34] T. Lopetegi, M. A. G. Laso, J. Hernandez, M. Bacaicoa, D. Benito, M. J. Garde, M. Sorolla, and M. Guglielmi, "New microstrip "wiggly-line" filters with spurious passband suppression," *IEEE Trans. Microwave Theory Tech.*, vol. 49, pp. 1593-1598, Sep. 2001.

[35] C. Quendo, J. Coupez, C. Person, E. Rius, M. Roy, and S. Toutain, "Band-pass filters with self-filtering resonators: a solution to control spurious resonances," in *IEEE MTT-S Symp. Dig.*, 1999, pp. 1135-1138.

[36] M. Makimoto and S. Yamashita, "Bandpass filters using parallel coupled stripline stepped impedance resonators," *IEEE Trans. Microwave Theory Tech.*, vol. 28, pp. 1413-1417, Dec. 1980.

[37] C. Wang and K. Chang, "Microstrip multiplexer with four channels for broadband system applications," *Int. J. RF Microwave CAE 11*, pp. 48-54, Nov. 2001.

[38] R. Mongia, I. Bahl, and P. Bhartia, *RF and Microwave Coupled-Line Circuits*, Boston: Artech House, 1999, pp. 371-372.